THE GEOLOGICAL SOCIETY OF AMERICA®

Linking metamorphism, magma generation, and synorogenic sedimentation to crustal thickening during Southern Appalachian mountain building, USA

H.H. Stowell[1], J.J. Schwartz[2], S.B. Ingram III[1], J. Madden[1], C. Jernigan[1], M. Steltenpohl[3], and P. Mueller[4]
[1]DEPARTMENT OF GEOLOGICAL SCIENCES, UNIVERSITY OF ALABAMA, TUSCALOOSA, ALABAMA 35487-0338, USA
[2]DEPARTMENT OF GEOLOGICAL SCIENCES, CALIFORNIA STATE UNIVERSITY–NORTHRIDGE, NORTHRIDGE, CALIFORNIA 91330, USA
[3]DEPARTMENT OF GEOLOGY, AUBURN UNIVERSITY, AUBURN, ALABAMA 36849, USA
[4]DEPARTMENT OF GEOLOGICAL SCIENCES, UNIVERSITY OF FLORIDA, GAINESVILLE, FLORIDA 32611, USA

ABSTRACT

The nature of metamorphism, magma compositions, the spatial distribution of plutons, and foreland sediments reflect, in part, the character and thickness of continental crust. We utilized metamorphic pressure-temperature-time (*P-T-t*) paths, garnet Sm-Nd ages, zircon U-Pb ages, and pluton compositions to estimate paleocrustal thickness and temporal changes in crustal magma sources in the Blue Ridge of the southernmost Appalachians. Garnet Sm-Nd ages for amphibolite-facies metamorphic rocks range from 331 ± 4 to 320 ± 3 Ma. Low- and high-Sr/Y plutons that intruded these metamorphic rocks have zircon U-Pb ages of 390 ± 1 to 365 ± 1 Ma and 349 ± 2 to 335 ± 1 Ma, respectively. Therefore, garnet growth began during regional metamorphism synchronous with or shortly after intrusion of the youngest high-Sr/Y trondhjemite plutons. Phase diagram sections and thermobarometry indicate that garnet growth initiated at ~5.8 kbar and 540 °C and grew during temperature increases of 60–100 °C and pressure increases of 2–3 kbar. The older, low-Sr/Y magmas are inferred to have been sourced in the crust at depths <~30 km, insufficient for garnet to be stable. However, the younger, high-Sr/Y magmas are inferred to have been sourced at >30 km depths where garnet was stable. Hafnium isotopic compositions for all the plutons, but one, exhibit a range from negative initial $\varepsilon_{Hf(i)}$ to weakly positive initial $\varepsilon_{Hf(i)}$, indicating incomplete mixing of dominantly crustal sources. Our data require minimum crustal thicknesses of ~33 km at 331 Ma; however, Alleghanian crustal thicknesses must have locally reached 39 km, based on crustal reconstruction adding the Alleghanian thrust sheet beneath the eastern Blue Ridge. We infer the presence of hot, tectonically thickened crust during intrusion of the early Alleghanian high-Sr/Y plutons and conclude that garnet growth and plutonism reflect a progressive increase in crustal thickness and depth of magma generation. The crustal thickening was synchronous with deposition of Mississippian to early Pennsylvanian sediments in the foreland basin of the Appalachian orogen between 350 and 320 Ma. This crustal thickening may have preceded emplacement of the Alleghanian thrust sheets onto the North American craton.

LITHOSPHERE; v. 11; no. 5; p. 722–749; GSA Data Repository Item 2019310 | Published online 14 August 2019 https://doi.org/10.1130/L1053.1

INTRODUCTION

Many collisional orogenic belts are intruded by paired magmatic belts that likely reflect spatial and temporal variation in magmatic sources; however, the processes by which and the tectonic settings in which these belts form are poorly understood (e.g., Tulloch and Kimbrough, 2003). They are typified by geochemically distinct suites of (1) mafic to felsic magmas with low Na, Al, and Sr, and high Y values (so-called "low-Sr/Y magmas"), and (2) less common, intermediate to felsic magmas with high Na, Al, and Sr, and low Y values (so called "high-Sr/Y magmas"). These high- and low-Sr/Y magmatic rocks are commonly distributed in margin-parallel, linear belts, and they constitute a largely unrecognized, but integral part of Phanerozoic convergent orogens worldwide. For example, paired high- and low-Sr/Y magmatic belts occur in the Tibetan Himalayas, Fiordland (South Island, New Zealand), the western U.S. Cordillera (Klamath Mountains, Blue Mountains Province), Peninsular Ranges, and the southern Appalachian orogen (Tulloch and Kimbrough, 2003; Chung et al., 2005, 2009; Xu et al., 2010; Schwartz et al., 2011; Zeng et al., 2011). One feature common to all of these paired magmatic belts is their association with contractional deformation in zones of crustal thickening. A key question in the development of paired magmatic belts is whether these belts form as a result of subduction-related processes, collisional processes, or other postsubduction lithospheric modification (e.g., delamination; Lee et al., 2006). Unraveling the interplay among magmatism, deformation, and crustal thickening in the development of paired magmatic belts is important in understanding how magmatism and melt generation operate and change in evolving orogenic belts.

The eastern Blue Ridge of the southern Appalachian orogen in Alabama provides a unique midcrustal window into the tectonic and magmatic evolution of a paired magmatic belt during convergent margin orogenesis. Previous workers have long recognized that plutonism associated with contractional deformation in the eastern Blue Ridge consisted of at least two distinct, magmatic suites distinguished by chemical composition and degree of deformation: (1) pre- to synkinematic Neoacadian, low-Sr/Y plutons, and (2) late- to postkinematic, high-Sr/Y plutons (Drummond et al., 1996). The origin of these two magmatic suites and their relationship to deformation

and metamorphism have largely remained enigmatic due in large part to limited geochronologic and petrologic data. Moreover, the processes that drove melt production at the southern termination of the Appalachian orogen also remain poorly understood, particularly with regard to postulated large-scale transport of terranes and crustal thickening processes.

Here, we investigated a section of the paired, high- and low-Sr/Y magmatic belts that crop out over the entire length of the eastern Blue Ridge and Inner Piedmont from Alabama to North Carolina (Fig. 1). We combined geochronology with igneous and metamorphic petrology in order to better understand the tectonic history, and the processes and timing of magma production in southernmost exposures of the magmatic belts. U-Pb zircon geochronology, whole-rock geochemistry, and zircon Lu-Hf isotope data analyses were applied to six intrusions that were emplaced over a period of more than 40 m.y. during and following Neoacadian deformation in the eastern Blue Ridge of Alabama. Garnet Sm-Nd geochronology, pressure-temperature (*P-T*) phase diagram sections (pseudosections), and thermobarometry were applied to the host metasedimentary rocks that were metamorphosed during this period. The southernmost exposures of the eastern Blue Ridge preserve a temporal transition from low-Sr/Y magmatism from 390 to 365 Ma to high-Sr/Y magmatism from 349 to 335 Ma. This transition occurred during and slightly preceding a period of regional amphibolite-facies metamorphism and contraction, which is recorded as a pressure increase of 2 to 3 kbar in garnet-bearing rocks of the eastern Blue Ridge in Alabama.

We found that Neoacadian contractional deformation locally resulted in crustal thickening of the eastern Blue Ridge to >35 km. This is compatible with the base of the crust locally having reached eclogite stability. Syncollisional, low-Sr/Y plutons emplaced in the eastern Blue Ridge of Alabama ca. 390–365 Ma were metamorphosed and deformed under amphibolite-facies conditions at midcrustal levels. Increases in crustal thickness beneath the eastern Blue Ridge resulted from synmetamorphic contractional and/or transpressional deformation, possibly involving collision with the Carolina terrane (Hatcher and Zeitz, 1980; Hibbard et al., 2002, 2007). Early metamorphism and low-Sr/Y magmatism were followed by deep-crustal (>35 km depth) partial melting from 349 to 335 Ma, leading to the construction of a geochemically distinct, high-Sr/Y magmatic belt. High-Sr/Y plutons display geochemical evidence for deep-crustal and possible mantle components. We propose that the pulse of high-Sr/Y magmatism during crustal thickening reflected increased magma source contributions from the lower lithosphere and/or asthenospheric mantle.

GEOLOGICAL SETTING

The Appalachians contain evidence for four Paleozoic orogenic events: Taconian, Acadian, Neoacadian, and Alleghanian. The Taconic orogeny began ca. 470 Ma in the southern Appalachians (Hatcher et al., 2007). Evidence for the Taconic event is well documented in the Blue Ridge of Tennessee, Georgia, and the Carolinas, but evidence for this event is limited in Alabama. The Acadian orogeny is defined as 410–380 Ma in the Northern Appalachians, and there is only limited evidence for the Acadian orogeny in the Southern Appalachians (e.g., Hatcher et al., 2007). In the Southern Appalachians, the Neoacadian orogeny began around 380 Ma and continued until the beginning of the Alleghanian orogeny ca. 325 Ma (Merschat et al., 2017). Alleghanian deformation, plutonism, and metamorphism extended until ca. 260 Ma. Complex overprinting of magmatism and metamorphism make delineation of the spatial and temporal boundaries between orogenies difficult.

The eastern Blue Ridge is a SW-NE–trending terrane located in the Southern Appalachian Mountains, stretching from Alabama to North Carolina. In Alabama, the eastern Blue Ridge is structurally bounded to the southeast by the Brevard fault, which separates the eastern Blue Ridge from the Inner Piedmont (Fig. 1). To the northwest, the Hollins Line fault separates the eastern Blue Ridge from the western Blue Ridge terrane, which is referred to as the Talladega slate belt in Alabama. Internally, the Blue Ridge is cut by the late Alleghanian (Tull, 1987) Alexander City and Goodwater-Enitachopco faults. The western and eastern Blue Ridge, and the Inner Piedmont are allochthonous and lie above the southern Appalachian master décollement, which has been identified in seismic data (Cook et al., 1979; Hopper et al., 2016). This subhorizontal fault, which underlies the eastern and western Blue Ridge and Piedmont, surfaces as the Talladega-Cartersville fault separating the western Blue Ridge rocks from passive-margin and Alleghanian foreland basin sedimentary rocks deposited on Laurentia (e.g., Cook et al., 1979; Tull, 1984). In Alabama, the foreland basin rocks include cyclic sediments of the Parkwood, Bangor Limestone, and Pottsville Formations of late Mississippian to Pennsylvanian age (Pashin, 1994). The Lower Pottsville Formation contains orogenic detritus from the Alleghanian orogenic core, indicating deposition during exhumation (Uddin et al., 2016). The older rocks and the foreland basin sedimentary rocks (e.g., Groshong et al., 2010) were deformed during Alleghanian deformation, which also transported crystalline rocks northwestward on the southern Appalachian master décollement (Hatcher, 1987, 1989, 2002, 2010).

Regional deformation in the eastern Blue Ridge and Inner Piedmont is characterized by shallowly to moderately dipping, NE-SW–oriented foliations, and shallowly plunging, NE-SW–trending lineations (e.g., Merschat et al., 2005; Huebner et al., 2017). Major NE-SW–striking, SE-dipping faults active during the Neoacadian event include the Hollins Line, Brevard, and Chattahoochee faults. Gastaldo et al. (1993) reported thrust stacking of the eastern Blue Ridge over the Talladega slate belt along the Hollins Line fault in post–early Mississippian time (ca. 360–345 Ma). Coeval deformation along the Brevard fault zone involved initial (360–350 Ma) NW-SE thrusting and development of shallowly to moderately dipping, NE-SW mylonitic foliations that later (ca. 330 Ma) transitioned into right-lateral shearing with top-to-the-SW movement (Vauchez, 1987; Vauchez et al., 1993; Hatcher, 2001; Merschat et al., 2005), coeval with contractional deformation along the Hollins Line fault. The ca. 335 Ma ductilely deformed Rabun pluton in western North Carolina is truncated by the Chattahoochee fault (Miller et al., 2006), indicating late Neoacadian thrusting. It is unclear whether Neoacadian deformation ca. 360–330 Ma resulted from a single protracted tectonic event, or episodic deformational pulses/events (Hatcher, 2010). The timing of metamorphism in the Blue Ridge of Alabama is constrained by $^{40}Ar/^{39}Ar$ cooling ages from the western Blue Ridge and eastern Blue Ridge (Steltenpohl, 2005), and by the Rb/Sr and U-Pb zircon ages of plutons (e.g., Russell et al., 1987; Tull et al., 2009). All of the pluton ages in the Blue Ridge are older than 340 Ma (Russell et al., 1987; Tull et al., 2009). The $^{40}Ar/^{39}Ar$ data from muscovite from the western Blue Ridge indicates cooling to Ar closure in muscovite at 334–320 Ma (McClellan et al., 2007). None of the published ages directly dates the thermal peak of metamorphism.

The southernmost exposures of the eastern Blue Ridge in Alabama are composed primarily of multiply deformed metasedimentary rocks, amphibolites, and metaplutonic rocks. The most extensive lithologic unit in the eastern Blue Ridge is the Wedowee Group, which is the host rock for all of the plutonic rocks of this study (Neathery and Reynolds, 1973). The Wedowee Group is structurally and stratigraphically(?) overlain to the southeast by the Emuckfaw Group (Fig. 1). The Wedowee Group ranges from low- to intermediate-grade quartzite, graphite-sericite-chlorite phyllite, and quartz-albite-muscovite-biotite schist to higher-grade garnet-biotite schist and garnet-biotite gneiss (Neathery and Reynolds, 1973). Most rocks exhibit a strong S_1 foliation and were affected by

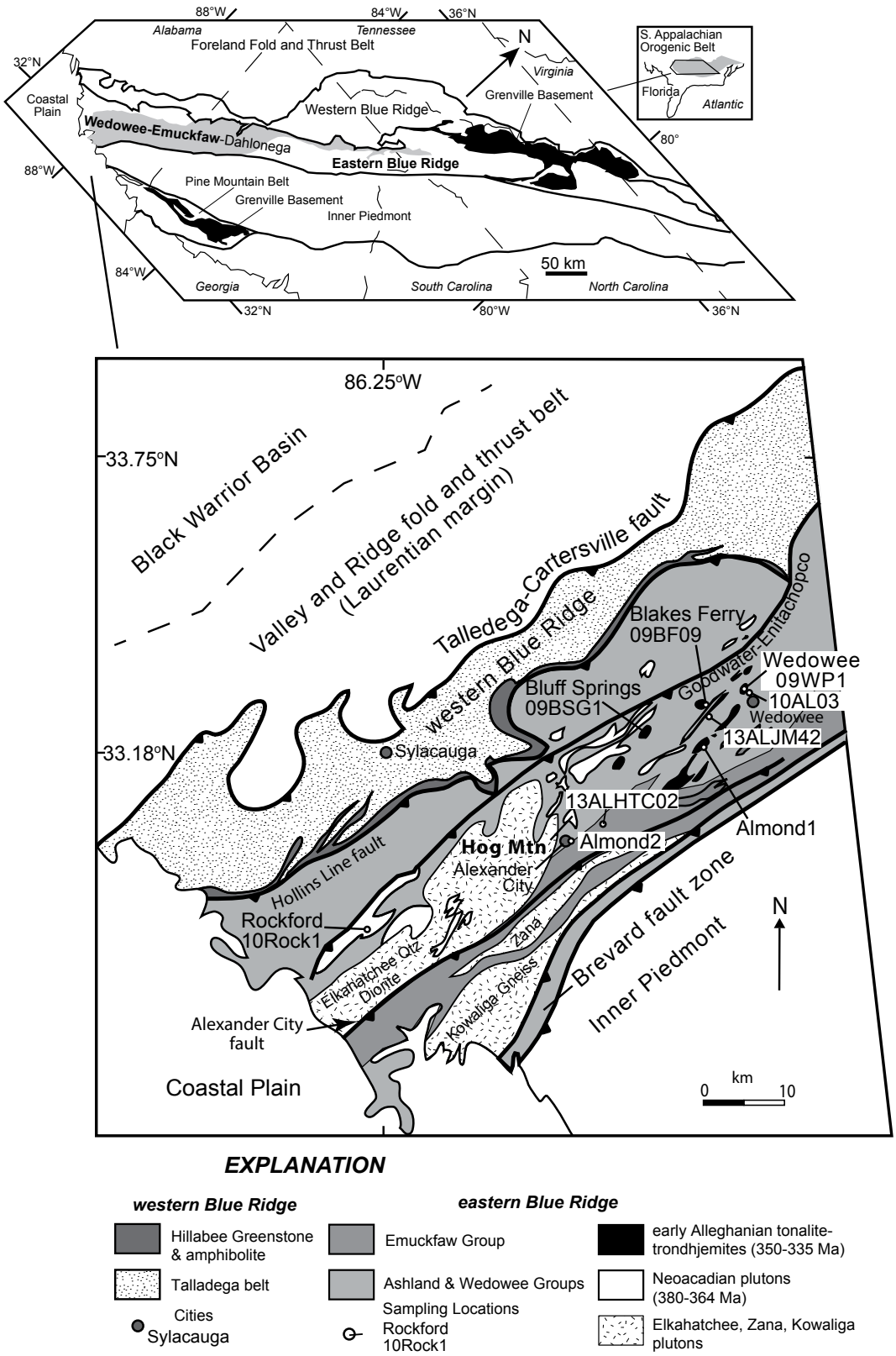

Figure 1. Simplified geologic map of the Blue Ridge in Alabama with Neoacadian and early Alleghanian plutons, and sample locations. Sample numbers preceded by names (e.g., Rockford) are plutonic rocks, and those without names are pelitic metasedimentary rocks. Figure is modified from McClellan et al. (2007) and Tull et al. (2014). Qtz—Quartz.

extensive, uniform regional metamorphism. Previous thermobarometic studies in the eastern Blue Ridge estimated regional metamorphic conditions of 580 °C ± 65 °C to 665 °C ± 50 °C and of 4.7 ± 1 to 8.5 ± 0.8 kbar from garnet-muscovite-biotite-plagioclase equilibrium (Gibson and Speer, 1986; Drummond et al., 1988; Stowell et al., 1996). Wedowee Group metasediments contain detrital zircon with a significant Grenville component and include mid-ocean-ridge basalt (MORB)–like metabasalts (Tull et al., 2014; Barineau et al., 2015). Tull et al. (2014) used these data to interpret the eastern Blue Ridge rocks as an Ordovician back-arc basin. The Emuckfaw Group, southeast of the Wedowee Group exposures (Fig. 1), is a sequence of garnet two-mica schist interlayered with garnet-biotite gneiss, micaceous quartzite, and amphibolite (Barineau et al., 2015). The lowermost Emuckfaw Group has been subdivided into the Josie Leg Formation, which includes coarse garnet two-mica, fine-grained biotite gneiss, and amphibolite. Barineau et al. (2015) interpreted the lower contact of the Josie Leg Formation with the uppermost Wedowee Group as a gradational stratigraphic contact.

Intrusive rocks of the eastern Blue Ridge typically occur as NE-trending, tabular, sill-like bodies. Plutons have been subdivided into groups that include: the Elkahatchee Quartz Diorite, the Zana and Kowaliga gneisses, the Bluff Springs Granite, the Rockford Granite, the Almond trondhjemites, the Hog Mountain Pluton, the Wedowee Pluton, and the Blakes Ferry Pluton. The batholith-scale Elkahatchee Quartz Diorite is the largest (~880 km^2) intrusion in the eastern Blue Ridge (Tull et al., 2009). U-Pb zircon for this body indicated an age range of 388–355 Ma (Steltenpohl et al., 2013; Barineau et al., 2015), compatible with a protracted intrusive history or possible metamorphic zircon growth. The dominant lithology is biotite-tonalite to granodiorite with subordinate diorite, granite, quartz monzonite, and trondhjemite. The Kowaliga and Zana gneisses (~510 km^2) range from tonalite to granodiorite (Drummond et al., 1997). Hawkins et al. (2013) reported U-Pb zircon dates of ca. 450 Ma for both of these units. The Hog Mountain Pluton, which has previously been dated by U-Pb zircon at ca. 384 Ma (Stowell and Odom Parker, 2015), is interpreted as a melt that formed as a result of basaltic underplating of thin continental arc crust (Green et al., 2015). The remaining plutonic rocks of the eastern Blue Ridge occur as small intrusions that range in size from <1.0 to 15 km^2, and they have been grouped based on spatial relations and composition. These small intrusions and nearby metamorphic rocks from the Wedowee Group (Fig. 1; Table 1) were the focus of this study and are discussed in more detail in the following sections.

Low-Sr/Y Granite Suite

The Rockford and Bluff Springs granite suites are peraluminous, muscovite-biotite granites with minor components of granodiorite, trondhjemite, and tonalite. These two suites typically exhibit a strong NE-SW–striking foliation (S_1) defined by planar alignment of muscovite-biotite and plagioclase feldspar. At map scale, these plutons are elongate parallel to the NE-SW trend of the orogen. The Rockford Granite has been the focus of numerous petrological, geochemical, and isotopic studies (e.g., Drummond et al., 1997). Most of the intrusion is medium-grained, hypidiomorphic, equigranular granite. Major minerals include quartz, plagioclase, K-feldspar, biotite, and muscovite; accessory phases include zircon, apatite, garnet, epidote, clinozoisite, and ilmenite. Biotite is the only mafic phase. Plagioclase typically displays a well-defined oscillatory normal zonation, but it also commonly displays evidence for subsolidus deformation with the development of subgrains. Whole-rock initial $^{87}Sr/^{86}Sr$ values from Russell et al. (1987) recalculated with $^{206}Pb/^{238}U$ zircon ages from this study ranged from 0.7055 to 0.7065 for the Rockford Granite, and from 0.7047 to 0.7069 for the Bluff Springs Granite. Russell et al. (1987) reported Rb-Sr whole-rock data for the Bluff Springs Granite indicating an age of 366 ± 21 Ma.

Drummond and Allison (1987) used major- and trace-element petrogenetic modeling of low-Sr/Y plutons to infer that the pre- to- synkinematic granites were associated with midcrustal partial melting of quartz-rich, water-saturated, peraluminous metasedimentary rocks in response to crustal shortening and regional metamorphism. The presence of primary muscovite requires ~9–10 wt% water at 4–5 kbar (Drummond and Allison, 1987). The Bluff Springs Granite is less studied; however, some consider it to be an along-strike continuum of the Rockford magmatism (Drummond et al., 1997). The much larger intrusive suite of the Elkahatchee Quartz Diorite has a mean Sr/Y value of 78 ± 50 (1σ) and $^{87}Sr/^{86}Sr$ value of 0.7036 (Drummond et al., 1997). The broad range in Sr/Y values encompasses values observed in both the low- and high-Sr/Y suites, and it is suggestive of a composite origin for the Elkahatchee Quartz Diorite. The wide range in apparent intrusive dates ranging from 388 to 355 Ma (Barineau et al., 2015) may also indicate a protracted emplacement history for the Elkahatchee Quartz Diorite.

High-Sr/Y Trondhjemite Suite

Petrologically and geochemically distinct trondhjemites in the Alabama eastern Blue Ridge have historically been termed "Almond trondhjemites" and include various elongate and circular (in map view) plutonic bodies. They are primarily biotite-muscovite trondhjemites and are typically mildly deformed to undeformed. Two larger bodies, the Wedowee and Blakes Ferry plutons, are circular intrusions of primarily biotite-muscovite trondhjemite that are mildly deformed and undeformed, respectively (Drummond et al., 1997). Typically, these trondhjemites are medium-grained intrusions with hypidiomorphic textures composed of plagioclase,

TABLE 1. SAMPLE LOCATIONS FROM THE EASTERN BLUE RIDGE, ALABAMA

Sample	Latitude* (°)	Longitude* (°)	Rock unit	Rock type	Location description
10ALHS03	33.32585	85.48279	Wedowee Group	Grt Bt Chl Ms phyllite	Lake Harris, north of Wedowee
13ALJM42A	33.27238	85.63083	Wedowee Group	St Grt Pl Bt Chl Ms phyllite	Lake Harris, south of Flat Rock
13ALHTC02	32.99252	85.84373	Emuckfaw Group	St Grt Pl Chlretro Bt Ms schist	Josie Leg Creek
10ALMOND1	33.14655	85.62093	Almond trondhjemite	Bt Ms trondhjemite	Town of Almond
10ALMOND2	32.91485	85.95113	Almond trondhjemite	Bt Ms trondhjemite	U.S. Route 280 & Alabama State Route 22
09BF09	33.28288	85.63728	Blakes Ferry Pluton	Bt Ms trondhjemite	Flat Rock Park, Lake Harris
09BSG1	33.16045	85.84126	Bluff Springs Granite	Bt Ms granite	CR-35 & Bluff Valley Road
10ROCK1	32.89396	86.22889	Rockford Granite	Bt Ms granite	Kings Bridge Road, 0.5 mi (0.8 km) NW of Rockford
09WP1	33.35241	85.45785	Wedowee Pluton	Bt Ms trondhjemite	APAC quarry, north of Wedowee

Note: Bt—biotite, Chl—chlorite, Grt—garnet, Ms—muscovite, Pl—plagioclase, St—staurolite.
*Datum is World Geodetic System 1984 (WGS84).

quartz, biotite, and muscovite with accessory minerals that include zircon, garnet, and titanite and secondary epidote, clinozoisite, and sericite. Strontium isotopic values from Russell et al. (1987) recalculated with $^{206}Pb/^{238}U$ zircon ages from this study yielded initial $^{87}Sr/^{86}Sr$ values that range from 0.7041 to 0.7054 for the Almond trondhjemites and from 0.7042 to 0.7044 for the Blakes Ferry pluton.

METHODS

Whole-Rock Analysis

Samples for whole-rock analysis were prepared by removing weathered fractions and then pulverizing representative splits with a C-steel ring and puck mill. Each of these powders were weighed and then dried at 1000 °C in a high-temperature oven. After drying, samples were reweighed to obtain loss on ignition values. Lithium borate flux was added to each sample at a ratio of 1:5. This mixture was melted in a platinum crucible and poured into a platinum mold to make glass discs. Selected trace elements were collected by analysis of pressed pellets. Powdered whole-rock samples were combined with a bonding agent and compacted with 5000 psi (34.5 bar) of pressure. Glass discs and pressed pellets were analyzed for major- and trace-element concentrations, respectively, on the PW2400 X-ray fluorescence (XRF) spectrometer at the University of Alabama. To ensure that precise concentrations were obtained from XRF analyses, each pressed pellet and glass disc was analyzed five times. The U.S. Geological Survey (USGS) andesite reference material AGV-1 was analyzed as an internal standard after every 10 unknowns. Average major-element oxide concentrations for AGV-1 and oxide concentrations for the Appalachian samples are presented in Table 2. XRF methodology, precision, and accuracy were described by Stowell et al. (2010).

Mineral Analysis

Quantitative mineral compositions and mineral zoning maps were obtained from individual point analyses and electron beam rastering, respectively. X-ray maps and quantitative point analyses were obtained

TABLE 2. REPRESENTATIVE COMPOSITIONS OF PELITIC AND GRANITIC ROCKS, EASTERN BLUE RIDGE, ALABAMA

	10ALHS03	13ALJM42A	13ALHTC02b	09BSG1	10ROCK1	09WP1	10ALMOND1	09BF09	AGV-1†	2σ (%Dif)§	AGV-1#
Major elements (wt%)											
SiO_2	57.57	57.78	66.24	67.97	67.06	69.28	72.60	67.99	59.88	0.46	60.07
TiO_2	1.39	1.15	0.83	0.16	0.28	0.07	0.07	0.09	1.08	0.02	1.07
Al_2O_3	23.18	21.25	17.12	19.03	17.49	18.91	15.28	19.67	17.63	0.28	17.51
Fe_2O_3	8.18	8.56	7.09	1.18	2.72	0.46	0.55	0.69	6.83	0.12	6.91
MnO	0.05	0.10	0.08	n.d.	0.06	b.d.	0.01	n.d.	0.10	0.00	n.d.
MgO	1.89	2.28	1.30	0.36	0.67	0.14	0.13	0.22	1.54	0.04	1.56
CaO	0.49	1.12	0.99	2.64	1.58	2.60	1.74	2.44	4.96	0.10	5.04
Na_2O	2.03	1.54	1.07	7.26	3.97	7.32	5.71	7.52	4.48	0.41	4.35
K_2O	4.46	4.01	3.30	1.47	4.21	1.25	2.00	1.43	3.00	0.05	2.98
P_2O_5	0.18	0.16	0.13	0.06	0.12	0.03	0.05	0.03	0.51	0.01	0.51
Total	99.43	97.92	98.15	100.12	98.17	100.05	98.12	100.07	100.00		100.00
Trace elements (ppm)											
V				88.4	28.8	16.4	29.4	14.2	125	7	121
Cr				39.6	0.4	b.d.	b.d.	b.d.	18	11	10
Ni				23.8	6.8	2.6	3.8	2.4	18	1	16
Cu				19.4	9.8	5.2	8.4	13.4	68	9	60
Zn				68.0	49.8	31.2	47.2	33.2	84	1	88
Rb				90.4	163.8	50.0	39.6	20.0	62	6	67
Sr				508.0	288.6	491.8	529.2	925.4	625	46	660
Y				18.0	18.2	7.4	6.2	1.8	20	1	20
Zr				192.8	120.4	107.4	152.2	155.6	267	25	227
Nb				7.8	9.6	3.8	4.2	2.2	17	8	15
Ba				743.6	880.6	592.0	434.4	501.8	1212	39	1230
La				28.1	21.6	10.7	16.7	6.9	48.2	27	38.0
Ce				47.8	40.1	18.9	34.8	11.9	77.3	15	67.0
Pr				5.6	5.9	2.2	4.1	1.4	8.3	9	7.6
Nd				21.1	22.9	8.4	16.0	5.2	31.0	6	33.0
Sm				3.8	4.0	1.8	0.5	1.0	5.0	15	5.9
Eu				1.2	0.8	0.5	2.7	0.5	1.4	14	1.6
Tb				0.2	0.5	0.2	0.2	0.1	0.7	0	0.7
Dy				1.0	3.2	0.9	1.3	0.3	3.9	7	3.6
Ho				0.3	0.6	0.2	0.2	0.1	0.7		n.d.
Er				0.5	1.6	0.4	0.6	0.1	1.8	6	1.7
Tm				0.1	0.3	0.1	0.1	0.0	0.3	20	0.3
Yb				0.5	1.7	0.3	0.5	0.1	1.5	10	1.7
Lu				0.1	0.2	0.0	0.1	0.0	0.3	7	0.3
Sr/Y*				28.2	15.9	66.5	85.4	514.1			
La/Yb				56.7	12.6	31.9	32.0	59.9			

Note: n.d. —not determined; b.d.—below detection limit.
†Average concentrations for AGV-1 U.S. Geological Survey (USGS) standard analyzed with PW2400 at the University of Alabama (UA), *N* = 10.
§Two sigma uncertainties for AGV-1 for major and select trace elements at UA. Rare earth element (REE) uncertainties are % difference between a single UA inductively coupled plasma–mass spectrometry analysis and accepted USGS values.
#USGS certificate concentrations.

on the JEOL 8600 electron probe microanalyzer (EPMA) at the University of Alabama following methods described by Stowell et al. (2010). The K_α X-ray maps were obtained using a Bruker energy-dispersive spectrometer and Esprit software. Quantitative point analyses were obtained using wavelength-dispersive spectrometers, CitZAF correction techniques, and Probe for EPMA software (Donovan, 2010). Major-element data for garnet and other phases were first qualitatively assessed with K_α X-ray maps and then quantified as appropriate with point analyses and line scans. Inclusions and compromised analyses were filtered out of the quantitative data. Additional information about EPMA methods and analytical precision at the University of Alabama can be found in Stowell et al. (2010). Select mineral compositions are reported in Table 3.

Samarium (Sm) and Neodymium (Nd) Isotope Analysis

Methods for garnet geochronology are modified from Stowell et al. (2010). Garnet-bearing samples were chosen in order to obtain >0.5 cm crystals with a minimal number of inclusions and relatively homogeneous matrix mineralogy. Sample preparation included drilling out select garnet grains with a drill press to separate garnet cores from whole grains. Whole or core/rim garnet pieces were crushed using a carbide steel mortar and pestle. Garnet fragments were first manually picked under a binocular microscope to avoid mineral inclusions. Additional inclusions were removed by leaching with HF and $HClO_4$ acid. The leached garnet was then fully dissolved in HF in SAVILLEX vials on a hot plate. Sample aliquots were spiked with mixed Sm and Nd Spike B from the University of North Carolina at Chapel Hill. Rare earth element (REE) fractions were separated and concentrated from samples using disposable polyprep Bio-Rad ion chromatography columns. Sm and Nd splits were separated from the REE fractions using methyllactic acid (MLA) and custom-designed 23 cm silica glass columns. Sm isotopes were measured as metal, and Nd isotopes were measured as oxide using a VG Sector 54 thermal ionization mass spectrometer (TIMS) at the University of North Carolina–Chapel Hill. Neodymium isotope ratios were normalized to $^{146}Nd/^{144}Nd = 0.7219$ and then used with Sm isotope values to compute final isotope ratios and elemental concentrations by isotope dilution. The JNdi Nd standard was run as an oxide periodically during the data collection with $^{143}Nd/^{144}Nd = 0.512117 \pm 0.000013$. Final Nd and Sm isotope ratios were plotted with Isoplot (Ludwig, 2012) to calculate isochron ages (Table 4).

Uranium (U) and Lead (Pb) Isotope Analysis

Approximately 3 kg aliquots of fresh rock were collected for each sample for zircon isotopic analysis, and zircon grains were extracted using standard mineral separation techniques. Following crushing, sample material was separated using a Gemini table. The heavy fraction of minerals was then separated using methylene iodide. Nonmagnetic zircon and monazite were separated using a Franz magnetic separator. Fifty to seventy inclusion-free zircon grains from each sample were handpicked under a binocular microscope and mounted in 2.4-cm-diameter epoxy disks with FC-1 and R33 zircon standards. Homogeneous zircon domains were identified from optical cathodoluminescence (CL) images. Backscattered-electron and CL images for monazite were obtained on the University of Alabama JEOL 8600 EPMA. In addition, select zircon grains were depth profiled after mounting them in indium in order to analyze overgrowths (rims). The CL images for zircon and backscattered-electron images for monazite are provided in the GSA Data Repository, in Figs. DR1 and DR2[1]).

U and Pb isotope data analysis of zircon and monazite in the Almond, Blakes Ferry, Bluff Springs, Rockford, and Wedowee samples was performed at the Stanford-USGS Micro-Analysis SHRIMP-RG (sensitive high-resolution ion microprobe–reverse geometry) facility. Epoxy mounts were gold coated to prevent charging during analysis. Spots for U-Pb analysis were chosen using reflected light and CL images based on zonation patterns. Rims and broad mantles of zircon were targeted, whereas inclusions and distinct cores were avoided. Samples were analyzed in two continuous sessions with standards run after every 3–4 unknowns. The primary O-ion beam generated analysis pits ~30 µm in diameter and ~2 µm deep, and sputtered secondary ions were mass analyzed in four cycles for each sample. These small pits allowed specific growth domains to be targeted. Fractionation of Pb relative to Th and U was corrected by comparison with the fractionation that occurred during analysis of the standard zircon. If common Pb corrections were needed, the Pb isotopic composition was based on the ^{204}Pb counts and estimated using the Stacey and Kramers (1975) models for average crustal Pb. Raw data were reduced onsite using the SQUID software (Ludwig, 2009), and all age calculations and concordia diagrams were made using IsoplotR (Vermeesch, 2018). Zircons with large common Pb corrections (e.g., analyses interpreted as having ~5% or greater contribution from common Pb) were discarded from further consideration. Zircon dates are reported using the $^{206}Pb/^{238}U$ age. In accordance with accepted norms, individual spot ages are reported in Table 5 with 1σ uncertainties and weighted averages for individual populations, and all ages in the text are presented with 2σ uncertainties and the mean square of weighted deviates (MSWD). An example of typical SHRIMP-RG precision and accuracy can be found in Eddy et al. (2019).

Hafnium (Hf) Isotope Analysis

Hf isotope ratios in zircon were obtained at the Department of Geological Sciences at the University of Florida, Gainesville, Florida, on a Nu-Plasma multicollector plasma-source mass spectrometer equipped with a New Wave UP-213 solid-state laser. In general, Lu-Hf spot analyses were chosen to overlap U-Pb SHRIMP-RG spots of magmatic growth domains, allowing correlation between zircon crystallization dates and Hf isotopic compositions. However, in the case of the Rockford Granite, U-Pb data were acquired after Lu-Hf measurements. Spots for Lu-Hf analysis were chosen from CL images based on grain zoning patterns, and distinct cores and inclusions were avoided. Data were acquired using a 40-µm-diameter spot size with static measurements of ^{180}Hf, ^{178}Hf, ^{177}Hf, ^{176}Hf, ^{175}Lu, ^{176}Lu, ^{174}Hf, ^{171}Yb, ^{172}Yb, and ^{173}Yb. Isobaric interference and mass bias corrections were conducted for each analysis on line and referenced to standard zircon FC-1 (Mueller et al., 2008). Hf isotope ratios and model ages are presented in Table 6. The FC-1 Duluth Gabbro zircon standard was analyzed periodically during the analytical sessions. The average $^{176}Hf/^{177}Hf$ value for these zircon was 0.28217 ± 0.00004 (2σ; $N = 13$, 1 outlier discarded) during the period of the analytical sessions.

Pressure and Temperature Estimation and Phase Diagram Models

Pressure and temperature estimates for metamorphism and pressure-temperature-time (*P-T-t*) paths for the eastern Blue Ridge rocks are from isochemical phase diagram sections (pseudosections) that were constructed in the 10-component MnO-Na_2O-CaO-K_2O-FeO-MgO-Al_2O_3-SiO_2-H_2O-TiO_2 (MnNCKFMASHT) chemical system. The fraction of

[1]GSA Data Repository Item 2019310, cathode luminescence (zircon) and backscattered electron images (monazite) of mineral grains dated by U-Pb, is available at http://www.geosociety.org/datarepository/2019, or on request from editing@geosociety.org.

TABLE 3A. GARNET COMPOSITIONS FROM THE EASTERN BLUE RIDGE, ALABAMA

Major elements (wt%)	10ALHS03		13ALJM42		13ALHTC01	
	Core	Rim	Core	Rim	Core	Rim
SiO_2	38.25	37.20	35.41	36.07	36.86	37.33
Al_2O_3	21.93	21.37	20.39	20.39	20.92	21.31
TiO_2	0.10	0.12	0.20	0.07	0.10	0.00
FeO^T	28.94	33.55	29.73	34.36	35.70	35.38
MgO	0.85	1.18	1.17	2.10	0.13	2.57
MnO	5.65	2.15	6.54	0.03	1.93	0.32
CaO	6.07	5.76	4.75	4.50	5.73	5.30
Total	101.79	101.34	98.12	97.54	101.36	102.20
Cations						
Si	3.016	2.973	2.943	2.985	2.975	2.953
Al	2.038	2.012	1.997	1.989	1.990	1.987
Ti	0.006	0.007	0.012	0.004	0.006	0.000
Fe^{+2}	1.909	2.241	2.066	2.378	2.410	2.340
Mg	0.099	0.141	0.145	0.259	0.015	0.303
Mn	0.377	0.146	0.460	0.002	0.132	0.021
Ca	0.513	0.494	0.424	0.400	0.496	0.449
Total	7.959	8.014	8.047	8.016	8.024	8.054
Mineral contents						
Mg#	0.049	0.059	0.066	0.098	0.006	0.115
Alm	0.658	0.742	0.668	0.783	0.789	0.751
Prp	0.034	0.047	0.047	0.085	0.005	0.097
Sps	0.130	0.048	0.149	0.001	0.043	0.007
Grs	0.177	0.163	0.137	0.132	0.162	0.144

Note: FeO^T—total iron; Mg#—Mg/(Mg + Fe); Alm—almandine; Prp—pyrope; Sps—spessartine; Grs—grossular.

(*continued*)

TABLE 3B. MICA COMPOSITIONS FROM THE EASTERN BLUE RIDGE, ALABAMA

Major elements (wt%)	10ALHS03		13ALJM42		12ALHS01	
	Bt	Ms	Bt	Ms	Bt	Ms
SiO_2	35.78	46.45	36.75	47.42	36.07	46.65
Al_2O_3	18.91	35.44	19.05	37.48	19.26	36.05
TiO_2	1.46	0.25	1.40	0.35	1.61	0.53
FeO^T	18.94	1.67	18.95	1.18	19.22	1.34
MgO	10.22	0.86	10.27	0.90	10.07	1.02
MnO	0.01	0.00	n.d.	n.d.	n.d.	0.00
CaO	0.00	0.03	0.01	0.01	0.00	0.01
Na_2O	0.21	1.16	0.24	1.07	0.17	1.36
K_2O	9.34	9.06	9.03	8.23	8.92	8.99
Total	94.85	94.92	95.69	96.65	95.33	95.94
Cations						
Si	2.725	3.086	2.760	3.064	2.726	3.063
Al	1.697	2.775	1.686	2.854	1.716	2.790
Ti	0.084	0.013	0.079	0.017	0.092	0.026
Fe^{+2}	1.206	0.093	1.190	0.064	1.215	0.073
Mg	1.160	0.085	1.150	0.087	1.135	0.100
Mn	0.001	0.000	n.d.	n.d.	n.d.	0.000
Ca	0.000	0.002	0.001	0.001	0.000	0.001
Na	0.031	0.149	0.035	0.134	0.025	0.173
K	0.907	0.768	0.865	0.678	0.860	0.753
Total	7.812	6.972	7.767	6.898	7.767	6.979
Mineral contents						
Mg#	0.490	0.478	0.491	0.576	0.483	0.577
Al IV	1.275	0.914	1.240	0.936	1.274	0.937
Al VI	0.422	1.862	0.447	1.918	0.441	1.853

Note: FeO^T—total iron; Al IV—tetrahedral Al; Al VI—octahedral Al; Bt—biotite; Ms—muscovite; n.d.—not determined.

(*continued*)

TABLE 3C. PLAGIOCLASE COMPOSITIONS FROM THE EASTERN BLUE RIDGE, ALABAMA

	10ALHS03	13ALJM42	13ALHTC01
Major elements (wt%)			
SiO_2	65.35	64.78	62.96
Al_2O_3	23.19	24.85	24.26
TiO_2	0.00	n.d.	0.00
FeO^T	0.05	0.24	0.00
MgO	0.00	n.d.	0.00
MnO	0.00	n.d.	0.00
CaO	4.23	4.15	5.43
Na_2O	7.62	8.37	6.81
K_2O	0.05	0.08	0.06
Total	100.49	102.46	99.51
Cations			
Si	2.847	2.774	2.779
Al	1.190	1.254	1.262
Ti	0.000	0.000	0.000
Fe^{+3}	0.000	0.019	0.000
Mg	0.000	n.d.	0.000
Mn	0.000	n.d.	0.000
Ca	0.198	0.191	0.257
Na	0.643	0.695	0.583
K	0.003	0.004	0.003
Total	4.881	4.939	4.884
Mineral contents			
Alb	0.762	0.781	0.691
An	0.234	0.214	0.305
Ksp	0.004	0.005	0.004

Note: FeO^T—total iron; Alb—albite; An—anorthite; Ksp—potassium feldspar; n.d.—not determined.

CaO in the whole rock, which is likely to be associated with phosphorus, was subtracted from the rock compositions assuming that all of the phosphorus is in stoichiometric apatite. All of the sections were constructed with THERIAK-DOMINO (de Capitani and Brown, 1987; de Capitani and Petrakakis, 2010), the Holland and Powell (1998) thermodynamic data set version 5.5 (November 2003), and whole-rock compositions following the methods in Stowell et al. (2010, 2014). Mineral activity models (chlorite, chloritoid, micas, ternary feldspar, garnet, amphibole, staurolite), and the THERIAK-DOMINO program were compiled by Doug Tinkham (Laurentian University). A summary of these solution models, their permitted site occupancies, and their source references were published by Gatewood and Stowell (2017). All other mineral phases were assumed to be pure. The water contents for isochemical *P-T* phase diagram sections were chosen to saturate all of the mineral assemblages that were modeled below the solidus.

RESULTS

Mineralogy and Garnet Zoning in Wedowee and Emuckfaw Samples

Wedowee Group garnet phyllite is characteristically muscovite rich with locally developed crenulation cleavage (e.g., Neathery and Reynolds, 1973). The samples collected for this study contained 4–10 mm near-euhedral garnet porphyroblasts in a matrix with sparse biotite and plagioclase. Schist from the Emuckfaw Group is coarser grained than Wedowee samples and locally contains ~15 mm subhedral garnet in a schistose matrix of muscovite and biotite.

Wedowee sample 10ALHS03 from ~3 km north of the town of Wedowee contained ~10 mm garnet in a matrix of fine-grained muscovite, chlorite, quartz, biotite, graphite, ilmenite, and tourmaline. A trace amount of fine-grained anhedral plagioclase was found in the sample. The muscovite-rich matrix defines a crenulated, phyllitic foliation (Fig. 2). Garnet is compositionally zoned with smoothly decreasing spessartine and smoothly increasing almandine from core to rim (Fig. 3). Pyrope and grossular show little variation across the grains; however, grossular shows small-scale oscillation and decreases toward the rim. We interpret this zoning to reflect garnet growth without modification by later processes.

TABLE 4. Sm AND Nd ISOTOPE RESULTS, EASTERN BLUE RIDGE, ALABAMA

Sample type/location	Weight (g)	[Sm] (ppm)	[Nd] (ppm	$^{147}Sm/^{144}Nd$	2σ	$^{143}Nd/^{144}Nd$	2σ	$^{143}Nd/^{144}Nd_i$ / $\varepsilon_{Nd}(t)$	2σ	Age (Ma ± 2σ)	MSWD	Prob.	*N*
Wedowee Gp. 10ALHS03													
Grt 1 rim	0.05443	0.728	0.128	3.4326	0.0248	0.518958	0.000041						
Grt 6 rim	0.04939	0.634	0.130	2.9615	0.0215	0.517938	0.000054						
MTX	0.15239	6.357	23.626	0.1626	0.0011	0.512098	0.000019			320 ± 3*	0.48	0.25	3 pt
Grt 6 core	0.05353	0.504	0.156	1.9532	0.0141	0.515888	0.000027						
Multi-Grt core	0.06510	0.651	0.239	1.6493	0.0117	0.515243	0.000037						
WR	0.15221	5.302	23.763	0.1349	0.0009	0.512105	0.000010	0.511707 / –6.9	0.000024 / 0.5	323 ± 3†	0.01	0.25	3 pt
Wedowee Gp. 13ALJM42A										331 ± 4	1.8	0.14	5 pt
Grt 1 core	0.05828	3.044	0.585	3.1518	0.0220	0.518650	0.000022						
Grt 1 rim	0.03597	1.049	0.212	2.9984	0.0222	0.518316	0.000014						
Multi-Grt rim	0.13399	0.920	0.270	2.0597	0.0153	0.516224	0.000024						
Grt 1 MTX	0.17479	7.503	39.116	0.1160	0.0008	0.512060	0.000010						
WR	0.17377	10.172	53.011	0.1160	0.0009	0.512055	0.000010	0.511713 / –6.7	0.000028 / 0.6				
Emuckfaw Gp. 13ALHTC02										330 ± 2	2.0	0.14	4 pt.
Grt core	0.04819	2.451	0.617	2.4040	0.0167	0.516787	0.000032						
Grt rim	0.05011	2.053	1.130	1.0991	0.0078	0.513965	0.000012						
MTX	0.14459	19.317	93.187	0.1253	0.0007	0.511860	0.000010						
WR	0.15839	27.843	134.282	0.1255	0.0010	0.511876	0.000012	0.511506 / –10.8	0.000093 / 1.8				

Note: Gp—Group. Initial $^{143}Nd/^{144}Nd$ and $\varepsilon_{Nd}(t)$ were calculated at 450 Ma because this is the inferred depositional age; see text for details. Grt—garnet, WR—whole rock, MTX—matrix (WR minus Grt), MSWD—mean square of weighted deviates.

*Grt rims were combined with MTX for age calculation.

†Grt cores were combined with WR for age calculation.

TABLE 5. U AND Pb ISOTOPE DATA AND AGES, EASTERN BLUE RIDGE PLUTONS, ALABAMA

Grain	Concentrations					Atomic ratios†						Age (Ma)		
	U (ppm)	Th (ppm)	Th/U	Pb§ (ppm)	*f*206# (%)	$^{238}U/^{206}Pb$††	% err (1σ)	$^{207}Pb/^{206}Pb$††	% err (1σ)	$^{206}Pb/^{238}U$§§	Abs. err. (1σ)	$^{206}Pb/^{238}U$##	Abs. err. (1σ)	Weighted average age (Ma ± 2σ)
Bluff Springs Granite														
BSG1-1	521	21	0.04	26.1	0.05	17.16	0.5	.0558	1.7	.0583	0.5	364	2	366 ± 1 Ma
BSG1-2.1	817	62	0.08	44.5	0.00	15.78	0.4	.0552	1.3	.0634	0.4	~~396~~	~~2~~	MSWD = 0.2
BSG1-3.1	518	17	0.03	25.4	0.05	17.49	0.5	.0546	1.8	.0572	0.5	~~358~~	~~2~~	*N* = 6
BSG1-4.1	690	56	0.08	34.7	0.14	17.10	0.4	.0541	1.4	.0585	0.4	366	2	
BSG1-5	479	56	0.12	24.0	0.00	17.12	0.5	.0536	1.7	.0584	0.5	366	2	
BSG1-6.1	569	60	0.10	28.0	0.09	17.47	0.5	.0539	1.6	.0572	0.5	~~359~~	~~2~~	
BSG1-7.1	486	30	0.06	24.4	0.00	17.12	0.5	.0554	1.7	.0584	0.5	365	2	
BSG1-8.1	444	5	0.01	22.4	0.00	17.05	0.6	.0566	1.8	.0587	0.6	366	2	
BSG1-9.1	601	99	0.17	30.1	0.00	17.15	0.5	.0536	1.5	.0583	0.5	365	2	
Rockford Granite														
ROCK1-1.1	610	331	0.54	31.7	0.04	16.53	0.5	.0544	1.4	.0605	0.5	379	2	390 ± 1 Ma
ROCK1-2.1	423	107	0.25	21.9	0.24	16.56	0.6	.0585	3.1	.0604	0.6	376	2	MSWD = 0.12
ROCK1-3.1	2154	106	0.05	116.2	0.02	15.92	0.3	.0541	0.8	.0628	0.3	~~393~~	~~1~~	*N* = 4
ROCK1-4.1	320	142	0.44	16.4	0.00	16.73	0.7	.0525	1.9	.0598	0.7	375	3	
ROCK1-5.1	2448	68	0.03	123.5	0.13	17.02	0.3	.0547	0.7	.0587	0.3	368	1	
ROCK1-6.1	2873	219	0.08	143.8	4.42	17.17	0.2	.0838	0.9	.0583	0.2	352	~~1~~	
ROCK1-7.1	2882	159	0.06	148.9	0.04	16.63	0.3	.0542	0.7	.0601	0.3	376	1	
ROCK1-8.1	1992	137	0.07	106.6	0.02	16.05	0.3	.0542	0.8	.0623	0.3	390	1	
ROCK1-9.1	2113	177	0.08	113.2	0.07	16.03	0.3	.0553	0.7	.0624	0.3	390	1	
ROCK1-10.1	5022	28	0.01	245.9	0.04	17.54	0.2	.0547	0.9	.0570	0.2	~~357~~	~~1~~	377 ± 2 Ma
ROCK1-11.1	742	115	0.16	39.6	0.11	16.09	0.5	.0530	1.3	.0621	0.5	389	2	MSWD = 0.6
ROCK1-12.1	3737	198	0.05	201.9	0.66	15.90	0.7	.0590	0.6	.0629	0.7	391	3	*N* = 4
Wedowee Pluton														
WP1-1	589	247	0.42	26.2	0.00	19.34	0.4	.0534	1.9	.0517	0.4	~~325~~	~~1~~	335 ± 1 Ma
WP1-2	549	126	0.23	25.3	0.13	18.61	0.5	.0535	1.4	.0537	0.5	337	2	MSWD = 5.9
WP1-3	1122	421	0.37	51.4	0.19	18.76	0.3	.0546	0.9	.0533	0.3	334	1	*N* = 7
WP1-4	576	109	0.19	26.7	0.06	18.52	0.4	.0528	1.3	.0540	0.4	339	1	
WP1-5	580	122	0.21	26.3	0.00	18.94	0.5	.0524	1.8	.0528	0.5	332	2	
WP1-6.1	517	114	0.22	23.8	0.11	18.68	0.5	.0534	1.7	.0535	0.5	336	2	
WP1-7.1	474	108	0.23	21.3	0.13	19.13	0.6	.0528	1.9	.0523	0.6	329	2	
WP1-8.1	1360	526	0.39	60.1	0.80	19.46	0.3	.0625	2.0	.0514	0.3	~~319~~	~~1~~	
WP1-9	427	104	0.24	19.3	0.00	19.01	0.6	.0539	2.0	.0526	0.6	330	2	
Almond trondhjemite (sample 1)														
ALMOND1-1.1	461	120	0.26	22.3	0.00	17.79	0.6	.0532	1.6	.0562	0.6	353	2	347 ± 2 Ma
ALMOND1-1.2	454	123	0.27	21.1	0.15	18.52	0.6	.0523	1.7	.0540	0.6	~~339~~	~~2~~	MSWD = 2.7
ALMOND1-1.3	393	113	0.29	18.7	0.22	18.03	0.6	.0516	1.7	.0555	0.6	349	2	*N* = 9
ALMOND1-1.4	452	134	0.30	20.4	0.00	19.08	0.6	.0525	1.8	.0524	0.6	330	2	
ALMOND1-1.5	287	75	0.26	12.8	0.00	19.28	0.9	.0538	2.1	.0519	0.9	326	3	
ALMOND1-1.6	369	86	0.23	17.4	0.14	18.23	0.6	.0541	1.8	.0549	0.6	344	2	
ALMOND1-1.7	702	181	0.26	32.4	0.09	18.61	0.5	.0533	1.3	.0537	0.5	~~337~~	~~2~~	
ALMOND1-1.8	425	106	0.25	19.9	0.00	18.30	0.6	.0533	1.8	.0547	0.6	343	2	
ALMOND1-1.9	638	58	0.09	29.8	0.05	18.37	0.5	.0544	1.4	.0544	0.5	341	2	
ALMOND1-1.10	424	87	0.21	20.4	0.25	17.89	0.6	.0536	2.1	.0559	0.6	351	2	
ALMOND1-1.11	396	105	0.26	19.4	0.00	17.59	0.6	.0534	1.8	.0569	0.6	~~357~~	~~2~~	

(*continued*)

TABLE 5. U AND Pb ISOTOPE DATA AND AGES, EASTERN BLUE RIDGE PLUTONS, ALABAMA (*continued*)

Grain	Concentrations					Atomic ratios†						Age (Ma)		
	U (ppm)	Th (ppm)	Th/U	Pb§ (ppm)	*f*206# (%)	$^{238}U/^{206}Pb$††	% err (1σ)	$^{207}Pb/^{206}Pb$††	% err (1σ)	$^{206}Pb/^{238}U$§§	Abs. err. (1σ)	$^{206}Pb/^{238}U$##	Abs. err. (1σ)	Weighted average age (Ma ± 2σ)
	Depth profile data													
ALMOND1-1.12	239	55	0.23	11.2	0.06	18.29	0.9	.0524	2.8	.0547	0.9	344	3	
ALMOND1-1.13	337	42	0.12	15.0	0.38	19.38	0.7	.0526	2.2	.0516	0.7	324	2	
ALMOND1-1.14	541	94	0.17	50.0	–0.04	9.31	0.6	.0693	3.8	.1075	0.6	652	4	
ALMOND1-1.15	350	10	0.03	15.3	–0.14	19.71	0.8	.0539	2.5	.0507	0.8	319	3	
ALMOND1-1.16	388	73	0.19	18.5	0.24	17.98	0.7	.0546	2.0	.0556	0.7	348	2	
ALMOND1-1.17	262	51	0.19	11.6	–0.05	19.44	1.0	.0524	3.1	.0515	1.0	324	3	
ALMOND1-1.18	252	58	0.23	11.1	–0.03	19.56	0.9	.0543	2.7	.0511	0.9	321	3	
ALMOND1-1.19	190	53	0.28	7.4	0.69	22.01	0.9	.0580	2.7	.0454	0.9	284	3	
ALMOND1-1.20	221	49	0.22	10.5	0.06	18.11	1.0	.0542	2.8	.0552	1.0	346	3	
ALMOND1-1.21	25	0	0.01	1.1	1.85	18.68	3.2	.0516	10.1	.0535	3.2	337	11	324 ± 2 Ma
ALMOND1-1.22	489	68	0.14	21.8	0.24	19.23	0.7	.0534	2.0	.0520	0.7	327	2	MSWD = 2.6
ALMOND1-1.23	261	66	0.25	11.4	0.57	19.70	0.9	.0519	3.9	.0508	0.9	320	3	*N* = 8
Almond trondhjemite (sample 2)														
ALMOND2-1.1	699	67	0.10	36.3	0.06	16.53	0.4	.0544	1.3	.0605	0.4	379	~~2~~	349 ± 2 Ma
ALMOND2-1.2	707	281	0.40	33.0	0.00	18.41	0.4	.0526	1.3	.0543	0.4	341	~~2~~	MSWD = 0.7
ALMOND2-1.3	712	268	0.38	32.5	0.10	18.84	0.5	.0536	1.4	.0531	0.5	333	~~2~~	*N* = 4
ALMOND2-1.4	974	166	0.17	45.3	0.33	18.46	0.4	.0557	1.4	.0542	0.4	339	~~1~~	
ALMOND2-1.5	831	126	0.15	37.2	10.28	19.18	0.6	.1307	4.7	.0521	0.6	297	~~3~~	
ALMOND2-1.6	799	233	0.29	37.4	1.10	18.32	0.4	.0634	2.8	.0546	0.4	338	~~2~~	
ALMOND2-1.7	1327	1054	0.79	59.9	1.14	19.04	0.3	.0611	1.0	.0525	0.3	327	~~1~~	
ALMOND2-1.8	1160	411	0.35	56.7	11.68	17.58	0.3	.1424	6.0	.0569	0.3	318	~~4~~	
ALMOND2-1.9	806	535	0.66	40.3	16.65	17.17	0.4	.1871	4.3	.0582	0.4	306	~~4~~	
ALMOND2-1.10	600	80	0.13	27.2	0.07	18.93	0.5	.0546	1.4	.0528	0.5	~~331~~	~~2~~	
ALMOND2-1.11	385	50	0.13	16.0	0.13	20.70	0.5	.0563	1.6	.0483	0.5	~~303~~	~~2~~	
ALMOND2-1.12	517	190	0.37	24.7	0.28	17.97	0.5	.0550	2.2	.0556	0.5	348	2	
	Depth profile data													
ALMOND2-1.13	261	107	0.41	11.0	0.17	20.33	0.9	.0545	2.7	.0492	0.9	~~309~~	~~3~~	
ALMOND2-1.14	595	186	0.31	25.9	0.07	19.74	0.6	.0546	1.7	.0506	0.6	~~318~~	~~2~~	
ALMOND2-1.15	196	32	0.16	17.9	1.68	9.38	0.9	.0770	2.0	.1066	0.9	~~641~~	~~6~~	
ALMOND2-1.16	656	41	0.06	31.4	0.33	17.97	0.6	.0586	1.8	.0556	0.6	347	2	
ALMOND2-1.17	1700	119	0.07	82.0	0.71	17.81	0.4	.0583	2.0	.0562	0.4	350	1	
ALMOND2-1.18	263	73	0.28	12.8	1.45	17.73	0.9	.0611	2.4	.0564	0.9	351	3	
ALMOND2-1.19	322	86	0.27	13.3	–0.02	20.74	0.8	.0560	2.4	.0482	0.8	~~302~~	~~2~~	
ALMOND2-1.20	438	141	0.32	19.0	0.61	19.85	0.7	.0612	2.0	.0504	0.7	~~314~~	~~2~~	
ALMOND2-1.21	298	71	0.24	13.5	1.08	19.00	0.8	.0626	2.3	.0526	0.8	~~327~~	~~3~~	

(*continued*)

TABLE 5. U AND Pb ISOTOPE DATA AND AGES, EASTERN BLUE RIDGE PLUTONS, ALABAMA (*continued*)

Grain	Concentrations					Atomic ratios†						Age (Ma)		
	U (ppm)	Th (ppm)	Th/U	Pb§ (ppm)	*f*206# (%)	$^{238}U/^{206}Pb$††	% err (1σ)	$^{207}Pb/^{206}Pb$††	% err (1σ)	$^{206}Pb/^{238}U$§§	Abs. err. (1σ)	$^{206}Pb/^{238}U$##	Abs. err. (1σ)	Weighted average age (Ma ± 2σ)
Blakes Ferry Pluton (zircon)														
BF09-1.1	1051	321	0.31	47.8	0.07	18.91	0.3	.0531	1.1	.0529	0.3	~~332~~	~~1~~	346 ± 1 Ma
BF09-1.2	1211	348	0.29	57.5	0.06	18.10	0.3	.0542	0.9	.0552	0.3	346	1	MSWD = 2.9
BF09-1.3	1628	451	0.28	74.9	0.35	18.66	0.3	.0562	0.8	.0536	0.3	~~335~~	~~1~~	*N* = 6
BF09-1.4	188	61	0.32	29.5	0.00	5.47	0.7	.0771	1.5	.1829	0.7	~~1081~~	~~7~~	
BF09-1.5	1675	495	0.30	79.9	0.01	18.00	0.3	.0542	0.8	.0555	0.3	348	1	
BF09-1.6	1497	468	0.31	70.6	0.03	18.21	0.3	.0535	0.9	.0549	0.3	345	1	
BF09-1.7	1430	458	0.32	67.5	0.02	18.19	0.2	.0530	0.8	.0550	0.2	345	1	
BF09-1.8	1200	457	0.38	53.8	0.11	19.15	0.3	.0535	0.9	.0522	0.3	~~328~~	~~1~~	
BF09-1.9	2117	860	0.41	98.2	0.07	18.52	0.2	.0538	0.7	.0540	0.2	~~339~~	~~1~~	
BF09-1.10	886	190	0.21	41.1	0.03	18.55	0.3	.0537	1.1	.0539	0.3	338	~~1~~	
BF09-1.11	1611	526	0.33	74.3	0.03	18.62	0.3	.0541	0.8	.0537	0.3	~~337~~	~~1~~	
BF09-1.12	1000	356	0.36	48.3	0.04	17.80	0.3	.0531	0.9	.0562	0.3	353	1	
BF09-1.13	847	144	0.17	39.0	0.10	18.64	0.5	.0536	1.2	.0536	0.5	~~337~~	~~2~~	
BF09-1.14	874	308	0.35	57.0	0.00	13.16	0.4	.0567	1.0	.0760	0.4	~~472~~	~~2~~	
BF09-1.15	738	100	0.14	106.6	0.00	5.95	0.3	.0725	0.7	.1682	0.3	~~1002~~	~~3~~	
BF09-1.16	552	113	0.20	25.9	0.05	18.32	0.5	.0519	1.5	.0546	0.5	343	2	
BF09-1.17	493	102	0.21	22.0	0.05	19.23	0.5	.0539	1.6	.0520	0.5	~~326~~	~~2~~	
BF09-1.18	409	34	0.08	19.0	0.14	18.50	0.7	.0551	2.0	.0541	0.7	~~339~~	~~2~~	
BF09-1.19	215	3	0.01	9.7	0.23	19.07	1.0	.0540	3.0	.0525	1.0	~~329~~	~~3~~	
BF09-1.20	488	57	0.12	22.0	0.41	19.08	0.7	.0551	2.1	.0524	0.7	~~328~~	~~2~~	
BF09-1.21	175	47	0.27	8.5	0.87	17.61	1.1	.0629	2.8	.0568	1.1	~~352~~	~~4~~	
BF09-1.22	253	17	0.07	10.7	0.74	20.30	1.0	.0593	2.8	.0493	1.0	~~308~~	~~3~~	
BF09-1.23	529	94	0.18	22.4	0.32	20.30	0.7	.0545	2.0	.0493	0.7	~~309~~	~~2~~	
Blakes Ferry Pluton (monazite)														
09BF1-1.1	471	20615	43.76	22.1	0.00	18.28	1.1	.0576	3.7	.0547	1.1	341	4	348 ± 3 Ma
09BF1-2.1	448	26537	59.25	21.0	0.17	18.34	1.1	.0548	3.0	.0545	1.1	342	4	MSWD = 2.0
09BF1-3.1	293	23332	79.74	14.4	0.00	17.46	1.4	.0594	3.6	.0573	1.4	357	5	*N* = 9
09BF1-4.1A	388	20436	52.69	17.3	0.00	19.24	1.3	.0549	3.3	.0520	1.3	~~326~~	~~4~~	
09BF1-5.1A	202	17356	86.09	9.4	0.55	18.35	1.7	.0581	4.5	.0545	1.7	340	6	
09BF1-6.1	384	22389	58.32	18.5	0.00	17.79	1.3	.0572	3.3	.0562	1.3	351	4	
09BF1-7.1	290	20673	71.33	13.8	0.52	18.11	1.6	.0535	3.8	.0552	1.6	346	6	
09BF1-8.1	300	23231	77.45	15.4	0.00	16.75	1.5	.0563	3.9	.0597	1.5	~~373~~	~~5~~	
09BF1-9.1	1018	24710	24.28	48.6	0.00	18.01	0.8	.0538	2.2	.0555	0.8	348	3	
09BF1-10.1	316	19349	61.21	15.3	0.00	17.70	1.6	.0600	4.4	.0565	1.6	352	6	
09BF1-11.1	249	25701	103.36	10.9	0.33	19.58	1.8	.0588	4.7	.0511	1.8	~~319~~	~~6~~	
09BF1-12.1	358	23402	65.44	17.6	0.00	17.44	1.3	.0552	3.4	.0573	1.3	359	5	

Note: Strikethrough indicates numbers that were not used for computing weighted means. All data were obtained by sensitive high-resolution ion microprobe–reverse geometry (SHRIMP-RG). MSWD—mean square of weighted deviates.

†Errors are reported at 1σ level and refer to last digits.

§Radiogenic ^{206}Pb.

#Fraction of total ^{206}Pb that is common ^{206}Pb.

††Uncorrected ratios.

§§^{207}Pb corrected ratios using age-appropriate Pb isotopic composition of Stacey and Kramers (1975).

##^{207}Pb corrected age; spot analyses with strikethrough were excluded in age calculation due to open-system behavior and/or analytical problems.

TABLE 6. Lu AND Hf ISOTOPE DATA FOR ZIRCON FROM PLUTONS IN THE EASTERN BLUE RIDGE, ALABAMA

Zircon	Volts Hf	Atomic ratios												
		$^{176}Hf/^{177}Hf$	1σ error	$^{176}Lu/^{177}Hf$	1σ error	$^{180}Hf/^{177}Hf$	1σ error	$\varepsilon_{Hf}(0)$	2σ error	$\varepsilon_{Hf}(t)^{\dagger}$	2σ error	T_{CHUR} (Ga)	T_{DM} (Ga)	$t(Ga)_{Zrn}$
Bluff Springs Granite														
BSG1-1	2.6	0.282621	0.000015	0.001200	0.000144	1.88650	0.00007	–5.8	1.1	2.0	1.4	0.27	0.88	0.36
BSG1-2.1	2.5	0.282378	0.000017	0.000230	0.000873	1.88662	0.00005	–14.4	1.2	–6.4	1.9	0.65	1.19	0.36
BSG1-3.1	2.6	0.282246	0.000015	0.000440	0.000527	1.88651	0.00007	–19.1	1.1	–11.1	1.5	0.86	1.37	0.36
BSG1-4.1	2.5	0.282425	0.000015	0.001000	0.000195	1.88675	0.00007	–12.7	1.1	–4.9	1.4	0.59	1.15	0.36
BSG1-5	2.1	0.282584	0.000015	0.000180	0.001627	1.88659	0.00008	–7.1	1.1	1.0	2.1	0.32	0.90	0.36
BSG1-6.1	2.1	0.282505	0.000022	0.000240	0.001086	1.88655	0.00008	–9.9	1.6	–1.9	2.3	0.45	1.01	0.36
BSG1-7.1	2.2	0.282448	0.000015	0.000490	0.000575	1.88681	0.00007	–11.9	1.1	–3.9	1.6	0.54	1.10	0.36
BSG1-8.1	1.9	0.282388	0.000029	0.001200	0.000244	1.88670	0.00010	–14.0	2.1	–6.2	2.4	0.65	1.20	0.36
BSG1-9.1	2.0	0.282561	0.000015	0.000190	0.001436	1.88665	0.00006	–7.9	1.1	0.1	2.0	0.36	0.94	0.36
Rockford Granite														
ROCK1-1.1	0.9	0.282453	0.000026	0.000260	0.003502	1.88664	0.00011	–11.7	1.8	–4.5	3.6	0.53	1.09	0.33
ROCK1-2.1	1.0	0.282500	0.000020	0.000420	0.001310	1.88647	0.00010	–10.1	1.4	–2.8	2.2	0.46	1.03	0.33
ROCK1-3.1	0.9	0.282501	0.000033	0.000280	0.002085	1.88612	0.00018	–10.0	2.3	–2.8	3.5	0.45	1.02	0.33
ROCK1-4.1	2.8	0.282454	0.000020	0.000130	0.002325	1.88675	0.00009	–11.7	1.4	–4.4	2.7	0.53	1.08	0.33
ROCK1-5.1	2.5	0.282524	0.000013	0.000170	0.001332	1.88678	0.00008	–9.2	0.9	–1.9	1.7	0.42	0.99	0.33
ROCK1-6.1	3.8	0.282465	0.000015	0.000130	0.002035	1.88667	0.00005	–11.3	1.1	–4.0	2.2	0.51	1.07	0.33
ROCK1-7.1	2.5	0.282496	0.000016	0.000130	0.001989	1.88651	0.00007	–10.2	1.1	–2.9	2.2	0.46	1.02	0.33
ROCK1-8.1	2.5	0.282561	0.000014	0.000160	0.002249	1.88664	0.00007	–7.9	1.0	–0.6	2.2	0.36	0.94	0.33
ROCK1-9.1	3.7	0.282460	0.000018	0.000090	0.004197	1.88658	0.00009	–11.5	1.3	–4.2	3.3	0.52	1.07	0.33
ROCK1-10.1	2.5	0.282374	0.000017	0.000560	0.000534	1.88672	0.00007	–14.5	1.2	–7.3	1.7	0.66	1.20	0.33
ROCK1-11.1	1.9	0.282582	0.000016	0.000190	0.001383	1.88667	0.00010	–7.2	1.1	0.1	2.0	0.32	0.91	0.33
ROCK1-12.1	2.1	0.282590	0.000016	0.000160	0.002041	1.88653	0.00007	–6.9	1.1	0.4	2.3	0.31	0.90	0.33
Wedowee Pluton														
WP1-1	2.8	0.282640	0.000017	0.000220	0.001599	1.88666	0.00008	–5.1	1.2	2.2	2.1	0.23	0.83	0.33
WP1-2	2.4	0.282667	0.000018	0.000250	0.001689	1.88668	0.00006	–4.2	1.3	3.1	2.2	0.19	0.79	0.33
WP1-3	2.9	0.282684	0.000015	0.000190	0.001341	1.88654	0.00007	–3.6	1.1	3.7	1.9	0.16	0.77	0.33
WP1-4	2.5	0.282659	0.000012	0.000160	0.001546	1.88670	0.00008	–4.5	0.8	2.9	1.8	0.20	0.80	0.33
WP1-5	2.7	0.282675	0.000017	0.000130	0.001882	1.88680	0.00008	–3.9	1.2	3.4	2.3	0.18	0.78	0.33
WP1-6	2.9	0.282646	0.000016	0.000150	0.001386	1.88651	0.00008	–4.9	1.1	2.4	2.0	0.22	0.82	0.33
WP1-7	2.3	0.282604	0.000013	0.000220	0.001014	1.88675	0.00007	–6.4	0.9	0.9	1.6	0.29	0.88	0.33
WP1-8	3.5	0.282630	0.000020	0.000190	0.002676	1.88656	0.00008	–5.5	1.4	1.8	2.8	0.25	0.84	0.33
WP1-9	1.9	0.282674	0.000017	0.000290	0.001396	1.88660	0.00010	–3.9	1.2	3.4	2.0	0.18	0.78	0.33
Almond trondhjemite (sample 1)														
ALMOND1-1.1	2.3	0.282488	0.000016	0.000200	0.000922	1.88681	0.00006	–10.5	1.1	–3.2	1.8	0.47	1.04	0.33
ALMOND1-4.1	1.5	0.282643	0.000019	0.000350	0.001355	1.88631	0.00009	–5.0	1.3	2.2	2.2	0.23	0.83	0.33
ALMOND1-5.1	1.3	0.282613	0.000020	0.000360	0.001153	1.88698	0.00009	–6.1	1.4	1.2	2.2	0.28	0.87	0.33
ALMOND1-6.1	1.3	0.282352	0.000025	0.001200	0.000408	1.88677	0.00010	–15.3	1.8	–8.2	2.2	0.71	1.25	0.33
ALMOND1-7.1	1.2	0.282490	0.000021	0.000250	0.001824	1.88670	0.00012	–10.4	1.5	–3.1	2.5	0.47	1.03	0.33
ALMOND1-8	0.9	0.282174	0.000033	0.000320	0.001856	1.88681	0.00012	–21.6	2.3	~~–14.3~~	~~3.4~~	0.97	1.47	0.33
ALMOND1-9	1.2	0.282489	0.000024	0.000240	0.001887	1.88657	0.00010	–10.5	1.7	–3.2	2.8	0.47	1.04	0.33
ALMOND1-10	1.2	0.282647	0.000026	0.000290	0.001459	1.88668	0.00010	–4.9	1.8	2.4	2.7	0.22	0.82	0.33
ALMOND1-11	1.1	0.282336	0.000039	0.001600	0.000410	1.88613	0.00009	–15.9	2.8	–8.9	3.2	0.75	1.29	0.33
Almond trondhjemite (sample 2)														
ALMOND2-1.1	3.0	0.282492	0.000013	0.000130	0.001422	1.88672	0.00006	–10.4	0.9	–3.0	1.8	0.47	1.03	0.33
ALMOND2-2.1	2.5	0.282284	0.000035	0.000280	0.000703	1.88679	0.00007	–17.7	2.5	~~–10.4~~	~~3.0~~	0.80	1.32	0.33
ALMOND2-4.1	3.2	0.282637	0.000011	0.000140	0.001364	1.88674	0.00005	–5.2	0.8	2.1	1.6	0.24	0.83	0.33
ALMOND2-6.1	3.0	0.282013	0.000016	0.000100	0.001873	1.88672	0.00007	–27.3	1.1	~~–20.0~~	~~2.2~~	1.22	1.68	0.33
ALMOND2-7.1	2.9	0.282590	0.000017	0.000180	0.001007	1.88666	0.00007	–6.9	1.2	0.4	1.9	0.31	0.90	0.33
ALMOND2-8.1	2.8	0.282664	0.000014	0.000160	0.001016	1.88667	0.00007	–4.3	1.0	3.0	1.7	0.19	0.79	0.33
ALMOND2-9.1	3.1	0.282491	0.000013	0.000110	0.001578	1.88654	0.00007	–10.4	0.9	–3.1	1.8	0.47	1.03	0.33
ALMOND2-10	2.8	0.282128	0.000018	0.000320	0.000695	1.88678	0.00006	–23.2	1.3	–16.0	1.8	1.05	1.53	0.33
ALMOND2-11	2.5	0.282333	0.000022	0.000390	0.000589	1.88657	0.00008	–16.0	1.6	–8.7	2.0	0.72	1.25	0.33
Blakes Ferry Pluton														
BF09-1	3.5	0.282680	0.000016	0.000160	0.000585	1.88643	0.00007	–3.7	1.1	–1.0	1.5	0.17	0.77	0.13
BF09-2	4.0	0.282644	0.000013	0.000210	0.000782	1.88666	0.00009	–5.0	0.9	2.3	1.5	0.23	0.82	0.33
BF09-3	3.6	0.282624	0.000016	0.000190	0.001060	1.88674	0.00006	–5.7	1.1	1.6	1.8	0.26	0.85	0.33
BF09-4	2.4	0.281877	0.000009	0.002900	0.000075	1.88676	0.00006	–32.1	0.6	~~–10.0~~	~~1.0~~	1.56	2.00	1.08
BF09-5	3.4	0.282377	0.000015	0.000550	0.000433	1.88665	0.00007	–14.4	1.1	–7.2	1.5	0.66	1.20	0.33
BF09-6	3.6	0.282558	0.000018	0.000250	0.000929	1.88666	0.00008	–8.0	1.3	–0.7	1.9	0.36	0.94	0.33
BF09-7	3.6	0.282664	0.000018	0.000210	0.000761	1.88662	0.00006	–4.3	1.3	3.0	1.8	0.19	0.80	0.33
BF09-9	3.0	0.282730	0.000013	0.000280	0.000500	1.88663	0.00008	–1.9	0.9	5.3	1.4	0.09	0.71	0.33
BF09-10	3.8	0.282733	0.000019	0.000300	0.001249	1.88673	0.00009	–1.8	1.3	5.4	2.1	0.08	0.70	0.33
BF09-11	2.2	0.282227	0.000016	0.001100	0.000278	1.88651	0.00010	–19.7	1.1	~~–12.6~~	~~1.5~~	0.91	1.42	0.33
BF09-12	2.6	0.282720	0.000014	0.000300	0.000729	1.88670	0.00006	–2.3	1.0	5.0	1.5	0.10	0.72	0.33
BF091-13	2.2	0.282318	0.000021	0.000490	0.000415	1.88666	0.00005	–16.5	1.5	–9.3	1.9	0.75	1.28	0.33
BF091-14	2.3	0.282457	0.000016	0.000210	0.001464	1.88659	0.00007	–11.6	1.1	–4.3	2.0	0.52	1.08	0.33
BF091-15	2.6	0.282167	0.000022	0.000280	0.000773	1.88662	0.00004	–21.9	1.6	~~–14.6~~	~~2.1~~	0.98	1.48	0.33
BF091-16	2.1	0.282242	0.000030	0.000850	0.000291	1.88660	0.00007	–19.2	2.1	~~–12.1~~	~~2.5~~	0.88	1.39	0.33
BF091-17	2.1	0.282278	0.000017	0.000460	0.000549	1.88662	0.00006	–17.9	1.2	~~–10.7~~	~~1.7~~	0.81	1.33	0.33

Note: Strikethrough indicates numbers that were not used for interpretations. Average $^{176}Hf/^{177}Hf$ for FC-1 Duluth Gabbro zircon was 0.28217 ± 0.00004 2σ (N = 13) during sample runs. T_{CHUR}—time of chondritic uniform reservoir separation; T_{DM}—time of depleted mantle separation; $t(Ga)_{Zrn}$—zircon age.

$^{\dagger}\varepsilon_{Hf}$ calculated at t = U-Pb zircon ages in Table 5.

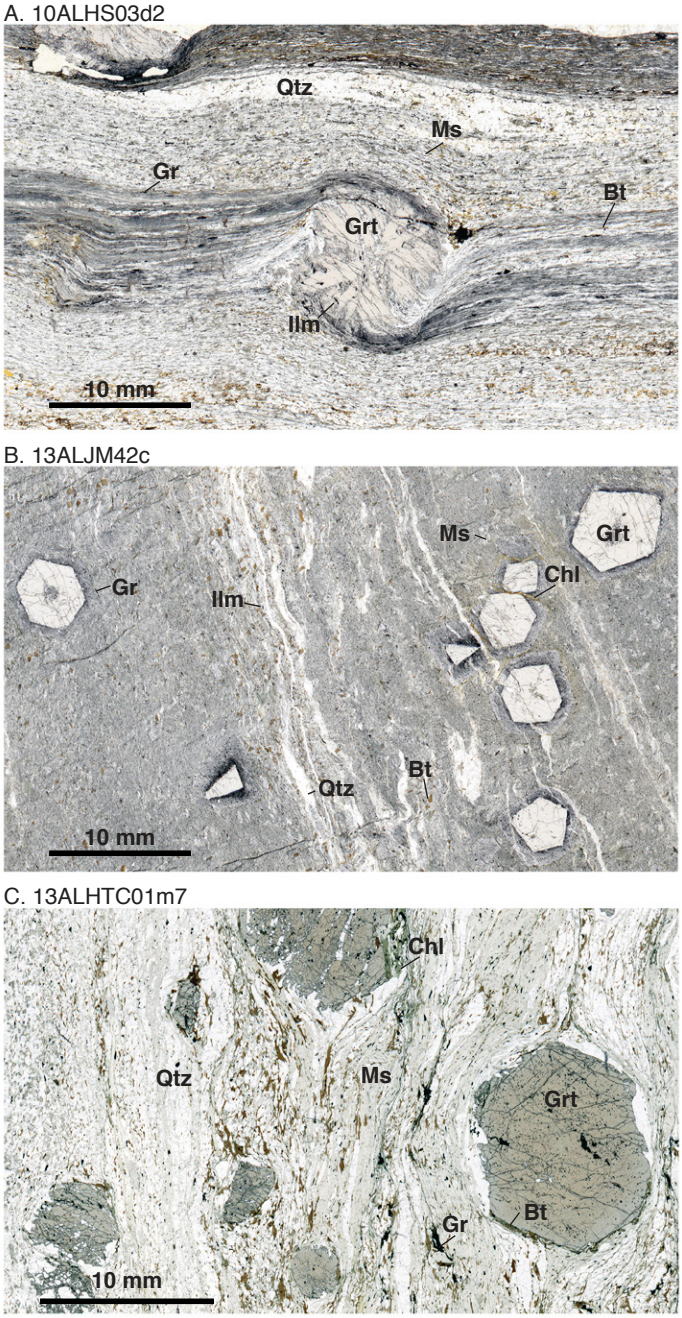

Figure 2. Photomicrographs of thin sections from samples of the Wedowee and Emuckfaw Groups, Alabama. (A) Garnet phyllite from the Wedowee Group, 10ALHS03. Note the large garnet porphyroblast with apparent rotation indicated by mineral alignment in pressure shadows and radial inclusions within garnet. (B) Garnet phyllite from the Wedowee Group, 13ALJM42. Note the euhedral garnet cores with few inclusions and the euhedral inclusion-rich rims. Only the outer-rim areas show evidence of growing over the foliation. (C) Emuckfaw Group schist, 13ALHTC02. Note the large subhedral garnet porphyroblasts with pressure shadows. The mineral textures in all samples indicate that much or all of the garnet grew prior to the last deformation. Bt—biotite, Chl—chlorite, Gr—graphite, Grt—garnet, Ilm—ilmenite, Ms—muscovite, Qtz—quartz, St—staurolite.

Wedowee sample 13ALJM42, ~7 km southwest of 10ALHS03, contained ~10 mm garnet in a matrix of fine-grained biotite, chlorite, muscovite, quartz, plagioclase, ilmenite, tourmaline, and graphite. The fine-grained matrix minerals define a schistosity with a crenulation cleavage (Fig. 2). Large chlorite porphyroblasts crosscut the foliation and are interpreted to have grown after peak metamorphism. Staurolite inclusions are found in the mantles of the large garnet porphyroblasts; however, no staurolite was found in central parts of garnet with highest Mn, and none was found in the matrix. This can be interpreted to indicate that temperatures increased to at least those of staurolite stability. Garnet is texturally and compositionally zoned, with euhedral cores with low inclusion density that are surrounded by broad rims that contain numerous inclusions of graphite, ilmenite, and quartz. Spessartine decreases and almandine and pyrope increase from core to rim (Fig. 3). Grossular is high in the core and rim, with a mantle of lower values between them. All of the end members show significant concentric variation with sharp changes on either side of the low grossular mantle; however, grossular has the greatest variation. We interpret this zoning to reflect garnet growth without modification by later processes. The low grossular mantle within these grains could result from growth of a high-Ca phase in the rock or an influx of low-Ca fluids. The possible explanations for grossular zoning are discussed in the modeling section below.

Emuckfaw sample 12ALHS01, from Josie Leg Creek northeast of Alexander City, contained ~12 mm garnet in a matrix of medium-grained biotite, chlorite, muscovite, quartz, plagioclase, rutile, and staurolite. A second sample (13ALHTC02) from Josie Leg Creek contained anhedral inclusion-rich and subhedral inclusion-poor garnet porphyroblasts (Fig. 2C). These <15 mm grains are in a matrix of muscovite, quartz, plagioclase, biotite, ilmenite, rutile, staurolite, and chlorite. Muscovite and biotite define a coarse schistosity with lenses and layers of quartz (Fig. 2). Staurolite is generally in a narrow area around the large garnet porphyroblasts, is not found as inclusions within garnet, and is interpreted to have grown during prograde partial consumption of garnet. Chlorite in this sample occurs locally as rims around garnet and as porphyroblasts crosscutting the fabric. It is interpreted as a product of late retrograde fluid infiltration. Garnet is compositionally zoned with decreasing spessartine, sharply decreasing grossular, and increasing pyrope core to near rim (Fig. 3). Almandine shows little variation but has a broad, low-amplitude mantle of higher values that correspond with a somewhat higher grossular mantle. There is a narrow (<0.5 mm) rim with a reversal in almandine and pyrope zoning. We interpret the majority of the garnet zoning to reflect growth, with the outermost area modified by diffusion.

Pressure-Temperature-Time Paths for Metamorphism

Three isochemical phase diagram sections constrain the peak *P-T*, *P-T* paths during garnet growth, and minimum crustal thicknesses during metamorphism in the eastern Blue Ridge of Alabama. The three *P-T* paths for Wedowee Group and Emuckfaw Group rocks indicate that garnet growth began at 540–550 °C at temperatures below predicted staurolite stability and that the pressure increased during garnet growth in all of these pelitic rocks (Fig. 4).

Initial garnet growth in Wedowee sample 10ALHS03 is predicted at 6 kbar and ~540 °C based on the intersection of core compositional isopleths (Fig. 4A). Garnet mode isopleths, the predicted plagioclase-absent fields in assemblages at higher *P* than core growth, the low abundance of plagioclase in the sample, and the orientation of garnet compositional isopleths indicate that garnet grew during increased *P*. A *P* increase is inferred because a steep *P-T* path with a positive slope is required in order to be subparallel to the pyrope and grossular isopleths (see Fig. 4A), resulting

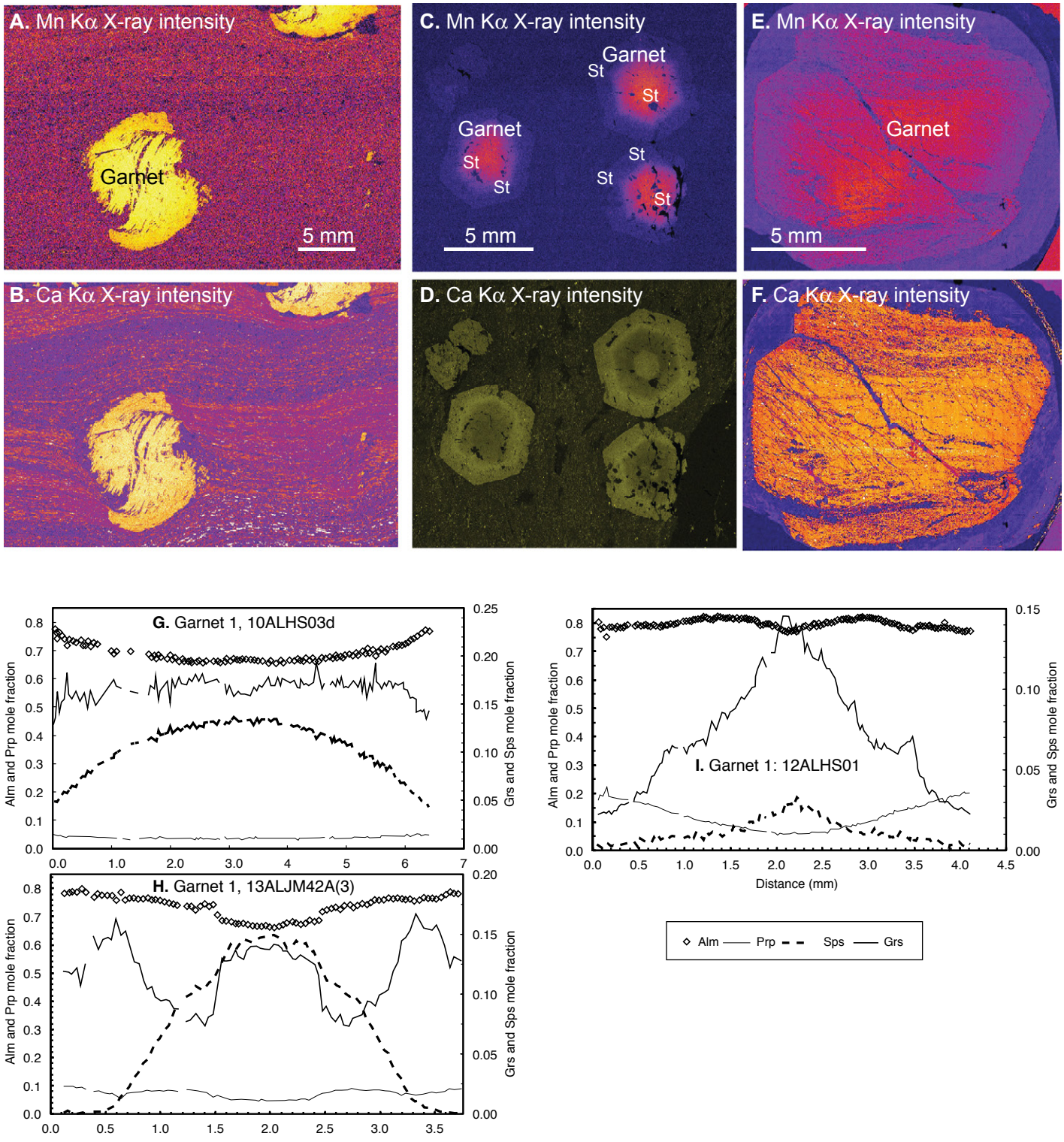

Figure 3. Compositions of garnet and adjacent minerals from samples in the Wedowee and Emuckfaw Groups, Alabama. (A) Manganese Kα X-ray intensity map, 10ALHS03. (B) Calcium Kα X-ray intensity map, 10ALHS03. (C) Manganese Kα X-ray intensity map, 13ALHS42. (D) Calcium Kα X-ray intensity map, 13ALHS42. (E) Manganese Kα X-ray intensity map, 13ALHTC02. (F) Calcium Kα X-ray intensity map, 13ALHTC02. (G) Mole fractions of end members along a line of analyses across garnet, 10ALHS03. (H) Mole fractions of end members along a line of analyses across garnet, 13ALHTC02. (I) Mole fractions of end members along a line of analyses across garnet, 13ALHTC02. Manganese zoning in all of the garnet is compatible with little or no diffusion within garnet and retention of growth zoning. See text for discussion of complex grossular zoning in 13ALJM42A. Alm—almandine, Grs—grossular, Prp—pyrope, Sps—spessartine, St—staurolite.

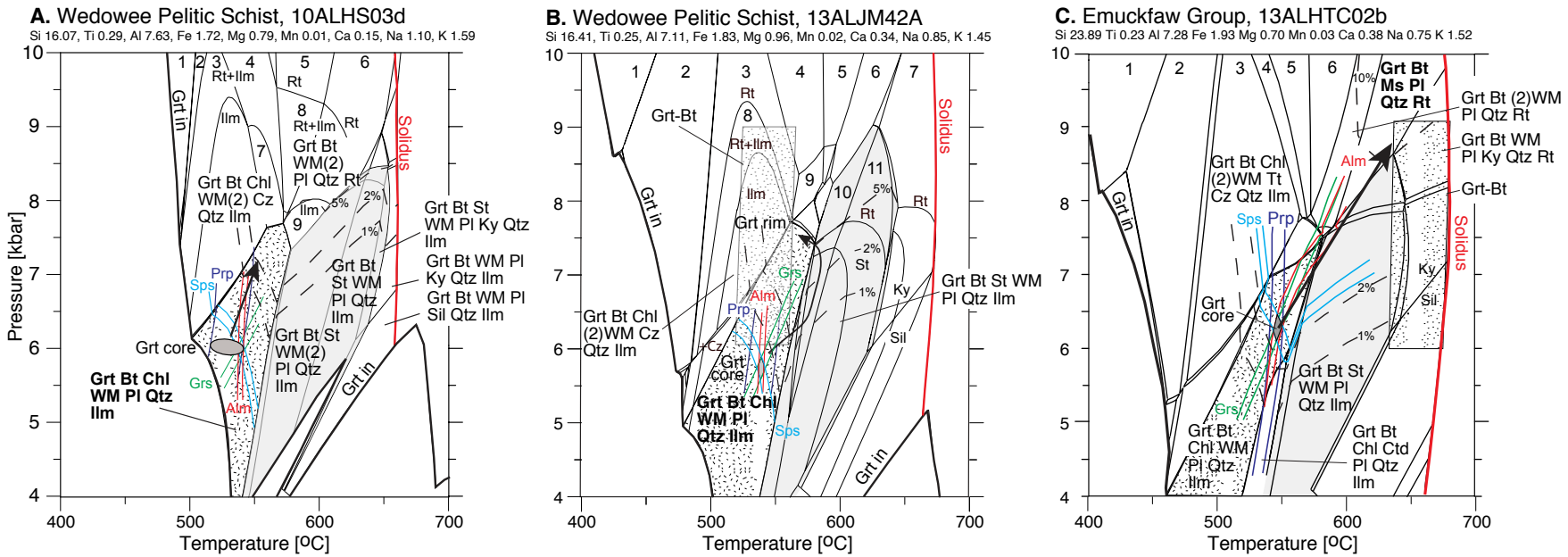

Figure 4. Pressure vs. temperature isochemical phase diagram sections (pseudosections) for metamorphic rocks in the eastern Blue Ridge, Alabama. (A) Garnet-bearing Wedowee Group pelitic phyllite from near the town of Wedowee, 10ALHS03. (B) Garnet-bearing Wedowee Group pelitic phyllite from near Harris Dam, 13ALJM42. (C) Garnet-bearing Emuckfaw Group pelitic schist from Josie Leg, 13ALHTC02. All mineral assemblages are plus H_2O. All of the staurolite-bearing mineral assemblages are shown in light gray. Alm—almandine, Amp—amphibole, And—andalusite, Bt—biotite, Chl—chlorite, Ctd—chloritoid, Cz—clinozoisite, Grs—grossular, Grt—garnet, Ilm—ilmenite, Ky—kyanite, Pl—plagioclase, Prp—pyrope, Qtz—quartz, Rt—rutile, Sil—sillimanite, Sps—spessartine, St—staurolite, WM—white mica. Isopleths for observed garnet core compositions are plotted in order to predict the pressure (*P*) and temperature (*T*) of garnet core growth. The inferred mineral assemblages during initial garnet growth are shown with a hatched pattern. The peak mineral assemblage field is indicated in bold. The peak temperatures for 13ALJM42 and 12ALHS01 (stippled pattern) were estimated from Fe-Mg exchange using garnet rim and biotite compositions and the calibration of Bhattacharya et al. (1992) over a range of 6–9 kbar. Uncertainties are plotted as ±25 °C. Numbered mineral assemblages in (A): 1 = Grt + Bt + Chl + 2WM + Qtz + Tt + Rt + H_2O; 2 = Grt + Bt + Chl + Cz + 2WM + Qtz + Tt + Rt + H_2O; 3 = Grt + Bt + Chl + Cz + 2WM + Qtz + Tt + Rt + Ilm + H_2O; 4 = Grt + Bt + Chl + 2WM + Qtz + Tt + Rt + Ilm + H_2O; 5 = Grt + Bt + 2WM + Qtz + Tt + Rt + H_2O; 6 = Grt + Bt + 2WM + Pl + Qtz + Tt + Rt + H_2O; 7 = Grt + Bt + Chl + 2WM + Qtz + Tt + Ilm + H_2O; 8 = Grt + Bt + 2WM + Qtz + Tt + Rt + Ilm + H_2O; 9 = Grt + Bt + 2WM + Qtz + Ilm + H_2O. Numbered mineral assemblages in (B): 1 = Grt + Chl + Cz + Amp + 2WM + Qtz + Tt + H_2O; 2 = Grt + Bt + Chl + Cz + 2WM + Qtz + Tt + H_2O; 3 = Grt + Bt + Chl + Cz + 2WM + Qtz + Rt + H_2O; 4 = Grt + Bt + Chl + 2WM + Qtz + Rt + H_2O; 5 = Grt + Bt + 2WM + Qtz + Rt + H_2O; 6 = Grt + Bt + 2WM + Pl + Qtz + Rt + H_2O; 7 = Grt + Bt + WM + Pl + Ky + Qtz + Rt + H_2O; 8 = Grt + Bt + Chl + Cz + 2WM + Qtz + Rt + Ilm + H_2O; 9 = Grt + Bt + Chl + Amp + 2WM + Qtz + Rt + H_2O; 10 = Grt + Bt + St + 2WM + Pl + Qtz + Rt + H_2O; 11 = Grt + Bt + St + WM + Pl + Qtz + Rt + H_2O. Numbered mineral assemblages in (C): 1 = Grt + Chl + Cz + Amp + 2WM + Qtz + Tt + H_2O; 2 = Grt + Bt + Chl + Cz + 2WM + Qtz + Tt + H_2O; 3 = Grt + Bt + Chl + 2WM + Qtz + Ilm + H_2O; 4 = Grt + Bt + Chl + 2WM + Qtz + Rt + Ilm + H_2O; 5 = Grt + Bt + Chl + 2WM + Qtz + Rt + H_2O; 6 = Grt + Bt + 2WM + Qtz + Rt + H_2O.

in garnet that lacks zoning in these components. The low abundance of plagioclase is compatible with a *P-T* path approaching the plagioclase mode zero line. The phase diagram section predicts a minimum pressure of 7 kbar for isothermal pressure increase to the peak assemblage; however, a *P-T* path that increases garnet mode to >2% garnet mode requires a pressure of 7.5–8 kbar (Fig. 4).

Garnet core growth in Wedowee sample 13ALJM42 is predicted at 5.6 kbar and 540 °C based on the core compositional isopleth intersection (Fig. 4B). Staurolite inclusions are found in the mantles of garnet, but they are not found in the garnet cores. Therefore, the presence of staurolite requires increasing temperature into the staurolite field during garnet growth. The lack of staurolite in the matrix could indicate that temperatures increased to those above staurolite stability. However, at near-constant *P*, this would stabilize kyanite or sillimanite with rutile and result in garnet resorption (see mode lines on Fig. 4B). The lack of aluminum silicates, absence of rutile and clinozoisite, lack of clear evidence for garnet resorption, and relatively low temperature prediction from garnet-biotite thermometry were used to infer a pressure increase at near-constant *T* (Fig. 4). The slope of the garnet mode isopleths in the staurolite field of the phase diagram indicates that increased *P* was required during garnet growth; therefore, final equilibration is interpreted to have been at ~7.5 kbar. The euhedral inner inclusion-poor and outer inclusion-rich zones of the garnet porphyroblasts, and the oscillation in Ca zoning could indicate a complex *P-T* path or a polyphase growth history. The simplest explanation, preferred here, is that the path crossed the grossular isopleths during increasing *T* and then again when *P* increased, causing large changes in the equilibrium Ca content.

Garnet core growth in Emuckfaw sample (13ALHTC02) is predicted at 6.3 kbar and 550 °C from the core compositional isopleth intersection (Fig. 4C). The rounded anhedral staurolite found in the matrix of the Emuckfaw samples from Josie Leg (12ALHS01 and 13ALHTC02) is interpreted to indicate garnet growth starting below staurolite stability followed by staurolite growth, and then resorption of staurolite. This is confirmed by garnet-biotite thermometry, which predicts temperatures above staurolite stability. We infer a *P-T* path of increasing temperature and pressure because increased *P* and *T* are required to reach the peak mineral assemblage field of garnet-biotite-muscovite-plagioclase-quartz-rutile. The *P* increase required to increase the garnet mode and stabilize rutile would be 2.5 to 3 kbar (Fig. 4C).

Crustal thicknesses were calculated assuming an average crustal density of 2750 kg/m^3, and the pressures determined from garnet core and rim compositions using isochemical phase diagram sections. These are all minimum crustal thickness estimates because garnet in all of the samples must have grown at or most likely considerably above the crust-mantle boundary. The estimated crustal thicknesses for initial garnet growth in samples 10ALHS03, 13ALJM42, and 13ALHTC02 are 22.2, 21.3, and 22.2 km, respectively. The estimated crustal thicknesses for rim garnet growth in samples 10ALHS03, 13ALJM42, and 13ALHTC02 are 26.7, 27.8, and 33.4 km, respectively. All of these estimates are for thickness during garnet growth; therefore, we cannot directly determine the crustal thickness prior to 330 Ma. However, we can document increased crustal thickness between 331 and 320 Ma.

Timing of Metamorphism

Garnet Sm-Nd ages constrain the timing of garnet growth and peak metamorphism. This is inferred from preserved growth zoning in major elements in garnet, which indicates that little or no diffusion occurred. Therefore, temperatures and heating durations could not have been sufficient for REE diffusion (e.g., Carlson, 2006, 2012).

One core and two rim aliquots were separated and handpicked from large (~0.8 cm) garnet grains in Wedowee sample 10ALHS03. An additional core aliquot was obtained from several additional garnet grains. Whole-rock and matrix (whole rock minus garnet) fractions close to the large garnet were chosen to complete the isotope data set (Table 4). The two garnet core and the whole-rock aliquots define a $^{143}Nd/^{144}Nd$ versus $^{147}Sm/^{144}Nd$ isochron with an age of 323 ± 3 Ma, MSWD = 0.006 (Fig. 5). The two garnet rim and the matrix aliquots define an isochron with an age of 320 ± 3 Ma, MSWD = 0.48 (Fig. 5). Using the upper and lower limits of age from the two sigma uncertainties, the garnet grew between 326 and 317 Ma.

One core aliquot and one rim aliquot were separated and handpicked from a large (~0.5 cm) garnet grain in Wedowee sample 13ALJM42a. An additional rim aliquot was obtained from several additional garnet grains. Whole-rock and matrix (whole rock minus garnet) fractions close to the large garnet were chosen to complete the isotope data set (Table 4). All of the garnet aliquots plus the whole rock and matrix define a $^{143}Nd/^{144}Nd$ versus $^{147}Sm/^{144}Nd$ isochron with an age of 331 ± 4 Ma, MSWD = 1.8 (Fig. 5). Therefore, the garnet most likely grew between 335 and 327 Ma, using the upper and lower limits of age from the two sigma uncertainties.

One core aliquot and one rim aliquot were separated and handpicked from a large (~1.0 cm) garnet grain in Emuckfaw sample 13ALHTC02b. Whole-rock and matrix (whole rock minus garnet) fractions close to the large garnet were chosen to complete the isotope data set (Table 4). All of the garnet aliquots plus the whole rock and matrix define a $^{143}Nd/^{144}Nd$ versus $^{147}Sm/^{144}Nd$ isochron with an age of 330 ± 2 Ma, MSWD = 2.0 (Fig. 5). Therefore, the garnet most likely grew between 332 and 328 Ma, using the upper and lower limits of age from the two sigma uncertainties.

Nd Isotopic Composition of Metasedimentary Rocks

The two whole-rock samples of the Wedowee Group and the single whole-rock sample of the Emuckfaw Group have Nd isotope compositions that help to constrain their provenance. The $\varepsilon_{Nd}(t)$ values for these rocks were calculated from the isotope data using t = 450 Ma. This 450 Ma approximate depositional age was based on a small number of detrital zircons collected in the Wedowee and Emuckfaw Groups and correlation of these rocks with Ordovician rocks in Georgia (Barineau et al., 2015). Wedowee Group $\varepsilon_{Nd}(t)$ values of −6.7 ± 0.6 and −6.9 ± 0.5 are indistinguishable from one another; however, the Emuckfaw Group $\varepsilon_{Nd}(t)$ value is distinct at −10.8 ± 1.8. For any age value younger than 1200 Ma, the calculated $\varepsilon_{Nd}(t)$ values are negative. Therefore, these rocks are clearly products of recycled crust and demonstrate little if any juvenile input.

Mineralogy and Geochemistry of Pluton Samples

The Neoacadian plutons are weak- to well-foliated, locally garnet-bearing granitic rocks. They are peraluminous, biotite-muscovite granites characterized by lower Sr/Y ratios (typically <40) relative to the early Alleghanian trondhjemites. The average Sr/Y value for the Rockford Granite is 15, whereas the average for the Bluff Springs Granite is 39 (Fig. 6). K_2O, MgO, and total Fe are enriched relative to the early Alleghanian high-Sr/Y trondhjemites (Ingram, 2012). In addition, V, Cr, Cu, Zn, Ni, Ba, Rb, and Y are enriched compared to early Alleghanian plutons (Table 2; Ingram, 2012). All Neoacadian samples are enriched in the light REEs relative to the heavy REEs, yet heavy REE concentrations are elevated compared to the early Alleghanian samples (Table 2; Ingram, 2012).

The early Alleghanian plutons are weak- to well-foliated, locally garnet-bearing trondhjemites. They are characterized by elevated Sr/Y

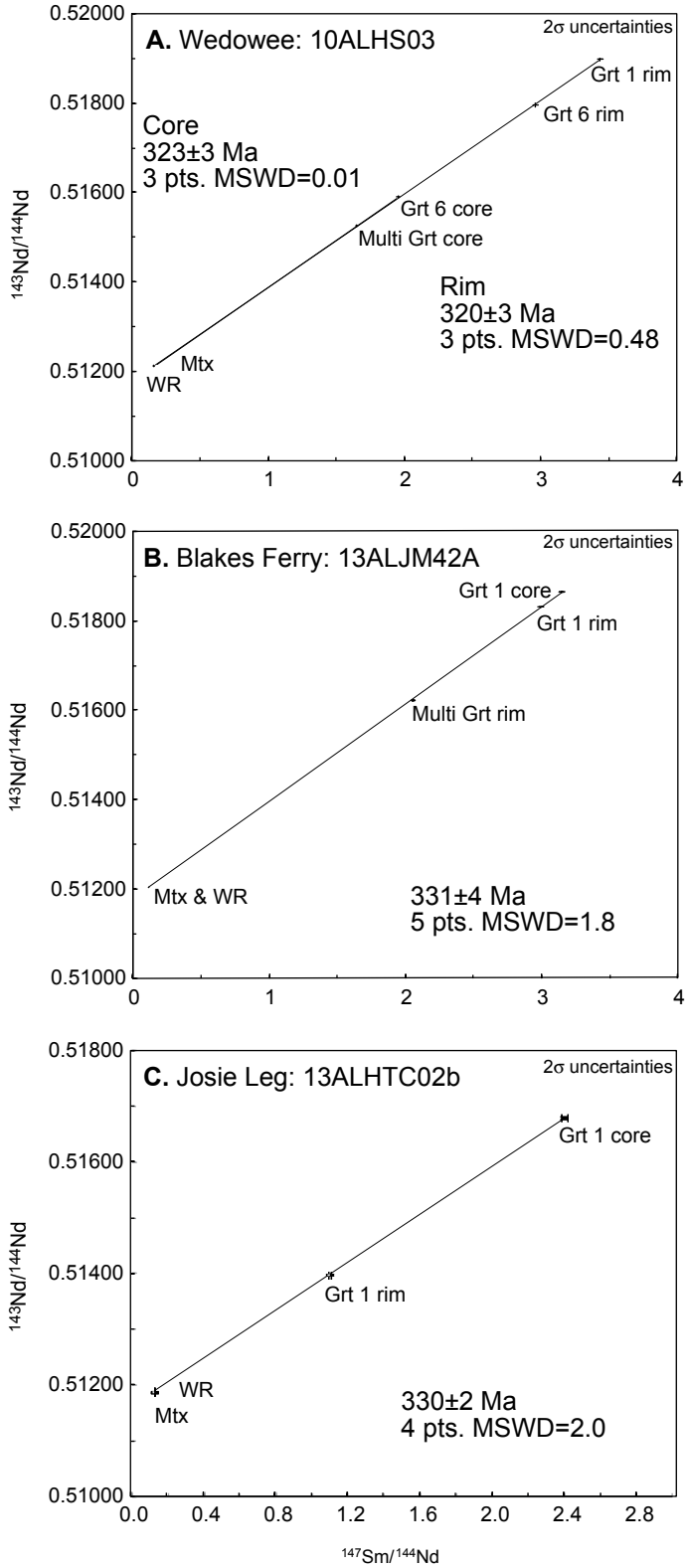

Figure 5. Garnet Sm-Nd rock isochrons for phyllite and schist from the eastern Blue Ridge in Alabama. (A) Wedowee sample 10ALHS03, Lake Harris near the town of Wedowee. Garnet cores and rims have different isotopic ratios, and separate ages are presented. (B) Wedowee sample 13ALJM42, Lake Harris near the Blakes Ferry Dam. Garnet core and rim isotopic values are not significantly different, and a single age is presented. (C) Emuckfaw sample 13ALHTC02, Josie Leg Creek near Alexander City. Garnet core and rim isotopic values are not significantly different, and a single age is presented. See Figure 1 for locations. MSWD—mean square of weighted deviates; Mtx—matrix; Grt—garnet; WR—whole rock.

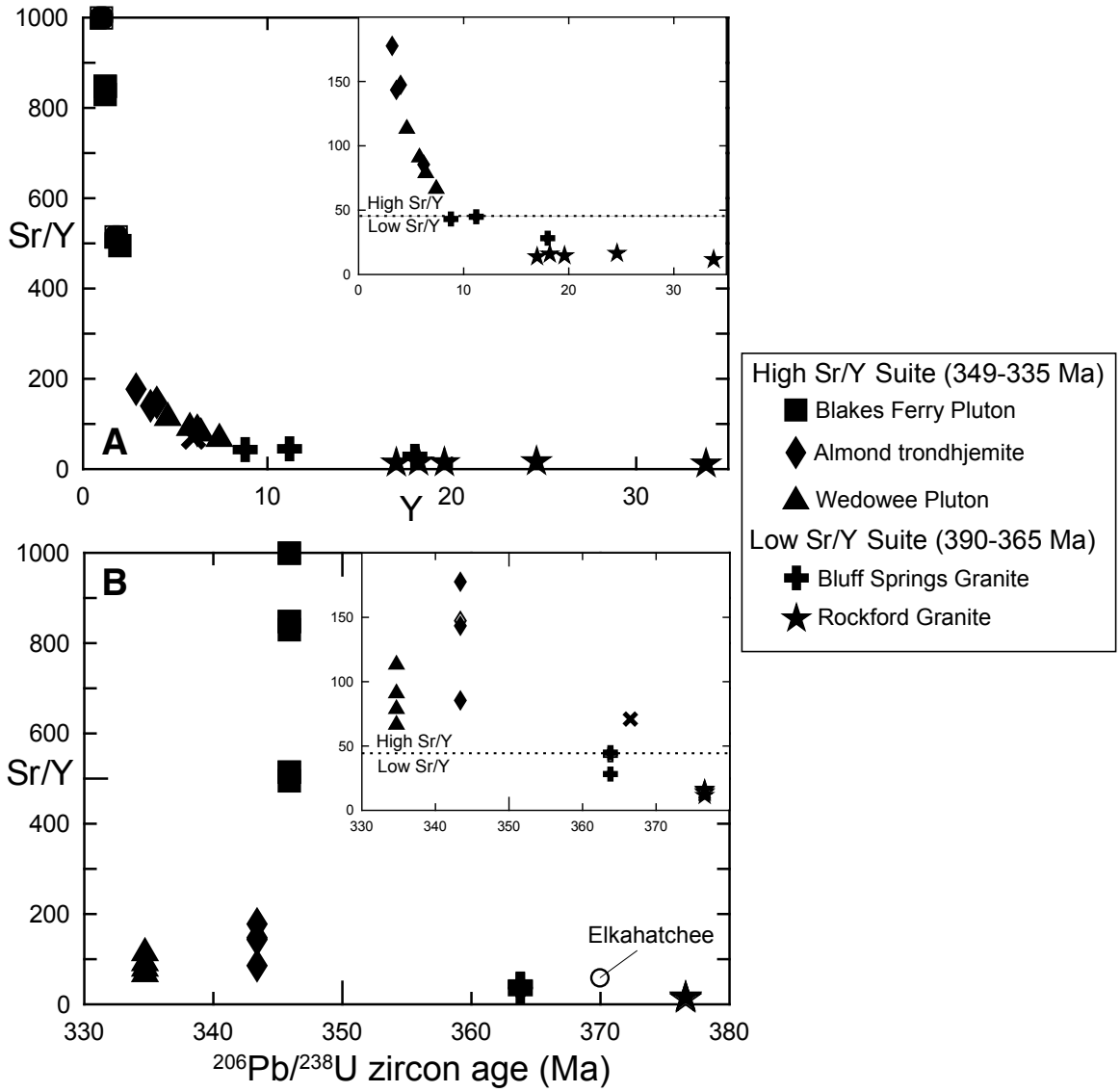

Figure 6. Strontium/yttrium plots for samples from Neoacadian and early Alleghanian plutons in the eastern Blue Ridge, Alabama. (A) Sr/Y vs. Y. (B) Sr/Y vs. $^{206}Pb/^{238}U$ zircon age. The Sr/Y ratio of 60.4 and age of ca. 370 Ma for the Elkahatchee Quartz Diorite are from Drummond et al. (1997) and Barineau et al. (2015), respectively.

ratios (>40) that range from 67 to 999 (Table 2). The average values for the Wedowee Pluton, the Almond trondhjemites, and the Blakes Ferry Pluton are 87, 138, and 737, respectively. Relative to the low-Sr/Y granites, the high-Sr/Y trondhjemites are peraluminous, high-SiO_2 plutons enriched in Na_2O and Sr. They rarely have detectable concentrations of MnO, Ni, and Cr. The early Alleghanian samples are enriched in the light REEs and highly depleted in the heavy REEs (Drummond et al., 1997; Ingram, 2012).

Timing of Plutonism

Low-Sr/Y Suite

Zircon grains in the Bluff Springs granite are typically stubby subhedral crystals. In CL, bright, low-U interiors are common, and many interiors lack distinct zoning, whereas other grains contain rounded, inherited cores typical of most eastern Blue Ridge plutons. Distinct growth zones are not well defined in the high-U, homogeneous, dark (in CL) rims (Fig. DR1). Nine of the thickest dark crystal tips and rims were chosen for analysis. One of these analyses, with a $^{206}Pb/^{238}U$ age of 396 Ma, was rejected as an outlier and is likely a xenocryst. The two youngest analyses of 358 and 359 Ma were rejected as outliers (Fig. 7A; Table 5), and the remaining six concordant analyses have an error-weighted average $^{206}Pb/^{238}U$ age of 365 ± 1 Ma with an MSWD of 0.2.

Zircon grains in the Rockford Granite are euhedral to subhedral, elongate prismatic crystals. In CL, distinct oscillatory zoning is present, and distinct euhedral oscillatory cores are common (Fig. DR1). Thin (<20 μm), dark rims were targeted for analysis, yet sampling of pure rim material was difficult due to their thin nature. Twelve grains have $^{206}Pb/^{238}U$ ages ranging from 393 to 352 Ma (Table 5). Nine concordant analyses (Fig. 7B) indicate two age populations that display error-weighted average $^{206}Pb/^{238}U$ ages of 390 ± 1 (MSWD = 0.12) and 377 ± 2 Ma (MSWD = 0.53). Both of these dates are geologically viable.

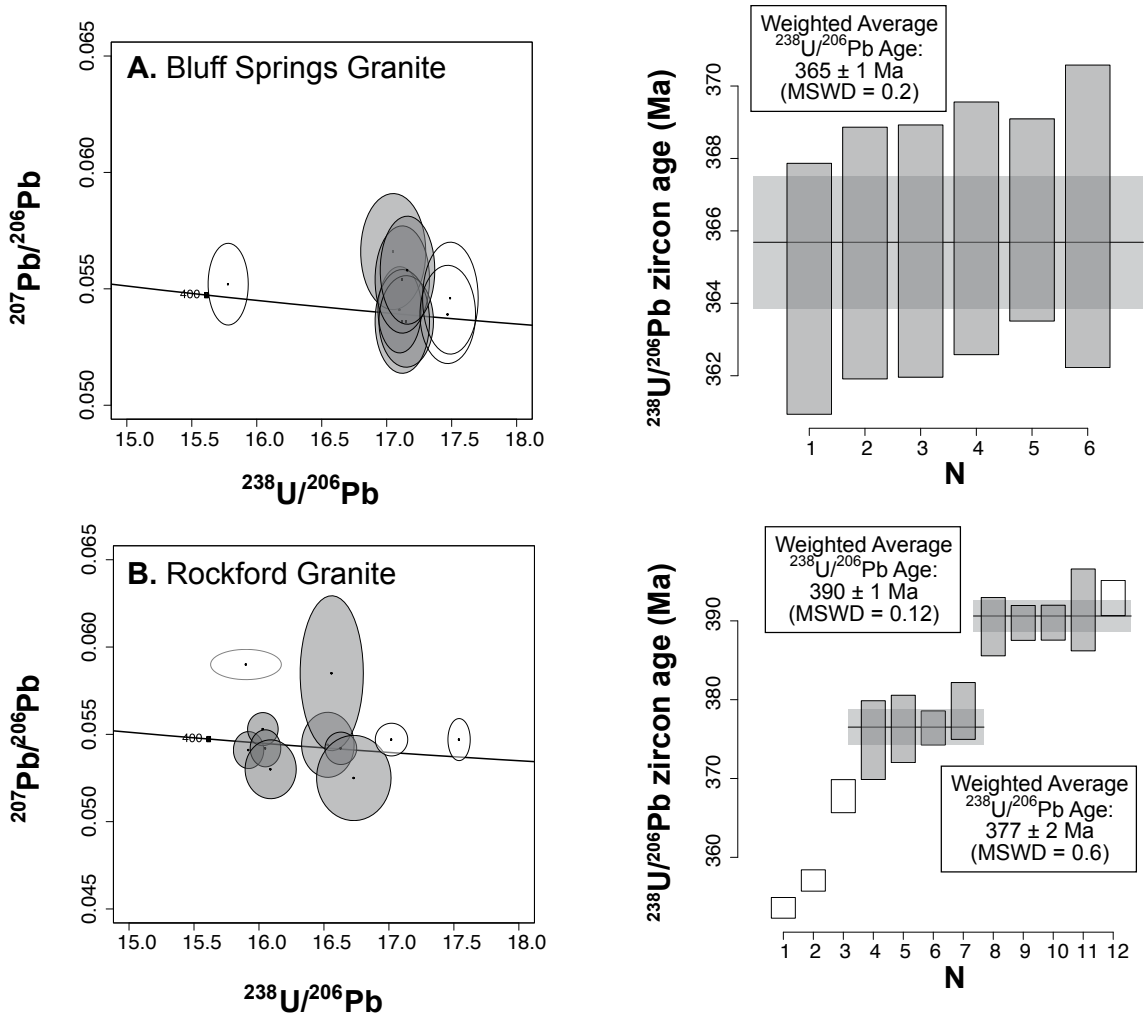

Figure 7. Tera-Wasserburg concordia plots and error-weighted average age plots for zircon in Neoacadian (ca. 390–365 Ma) low-Sr/Y plutons in the eastern Blue Ridge. (A) Bluff Springs Granite. (B) Rockford Granite. Note two distinct age populations in the Rockford sample. All U-Pb ages for both plutons are plotted with 2σ uncertainties, and all calculated ages are listed as ±2σ. Ages used to calculate the weighted means are shown as gray ellipses on the Tera-Wasserburg concordia plots. U and Pb isotope data can be found in Table 5. MSWD—mean square of weighted deviates.

High Sr/Y Suite

Zircon grains from the undeformed Wedowee Pluton are elongate, yet stubby in nature with bright subhedral to rounded cores in CL (Fig. DR1). Most of the overgrowths surrounding these cores are dark gray to black in CL with indistinct to faint zoning. Late-stage zircon growth is represented by moderately thick overgrowths (~30 µm), which were targeted for analysis. The nine grains selected have $^{206}Pb/^{238}U$ ages ranging from 339 to 320 Ma (Table 5). Most of the ages are concordant, and only two analyses were rejected on the basis of discordance to yield an error-weighted average $^{206}Pb/^{238}U$ age of 335 ± 1 Ma with a high MSWD of 5.9 (Fig. 8A).

Zircon grains from each of the two Almond trondhjemite samples were similar in morphology and characterized by distinct, oscillatory zoning that typically surrounded rounded, xenocrystic cores (Fig. DR1). Most grains had thin (<10 µm), high-U rims. SHRIMP-RG dating targeted these rims in grain mount and via depth profiling. Grain mount results for 10ALMOND1 yielded $^{206}Pb/^{238}U$ dates ranging from 357 to 326 Ma for 11 analyses (Table 5). The results of the depth profiling are far more complicated, with dates ranging from 348 to 284 Ma (Table 5). Seven of the 12 depth profiling analyses resulted in $^{206}Pb/^{238}U$ ages less than 330 Ma. In Tera-Wasserburg space, data cluster in two distinct populations and yield error-weighted average ages of 324 ± 2 Ma (MSWD = 2.6) and 347 ± 2 (MSWD = 2.7; Fig. 8B). The results from 10ALMOND2 are similar to those of 10ALMOND1, yet they display an even greater age range. The analyses of these zircon resulted in a range of 379–296 Ma, whereas the range of age from the depth profiling is 351–302 Ma (Table 5). Four of the oldest analyses yielded an error-weighted average $^{206}Pb/^{238}U$ age of 349 ± 2 Ma, MSWD = 2.6 (Fig. 8C).

Twenty-three zircon and 12 monazite grains from the Blakes Ferry Pluton were analyzed. Zircon grains occur as two distinct morphologies (Fig. DR1). The first population consists of elongate (~200 µm), rounded to subhedral grains. Light gray to white cores in some grains often exhibit oscillatory zoning. In some grains, these low-U cores dominate the entire crystal, and these grains were not chosen for analysis. In some dark (CL) grains, high-U, magmatic overgrowths appear almost homogeneous, yet subtle zoning can be found in some rims. The second population is similar to other samples in this study and is characterized by rounded cores surrounded

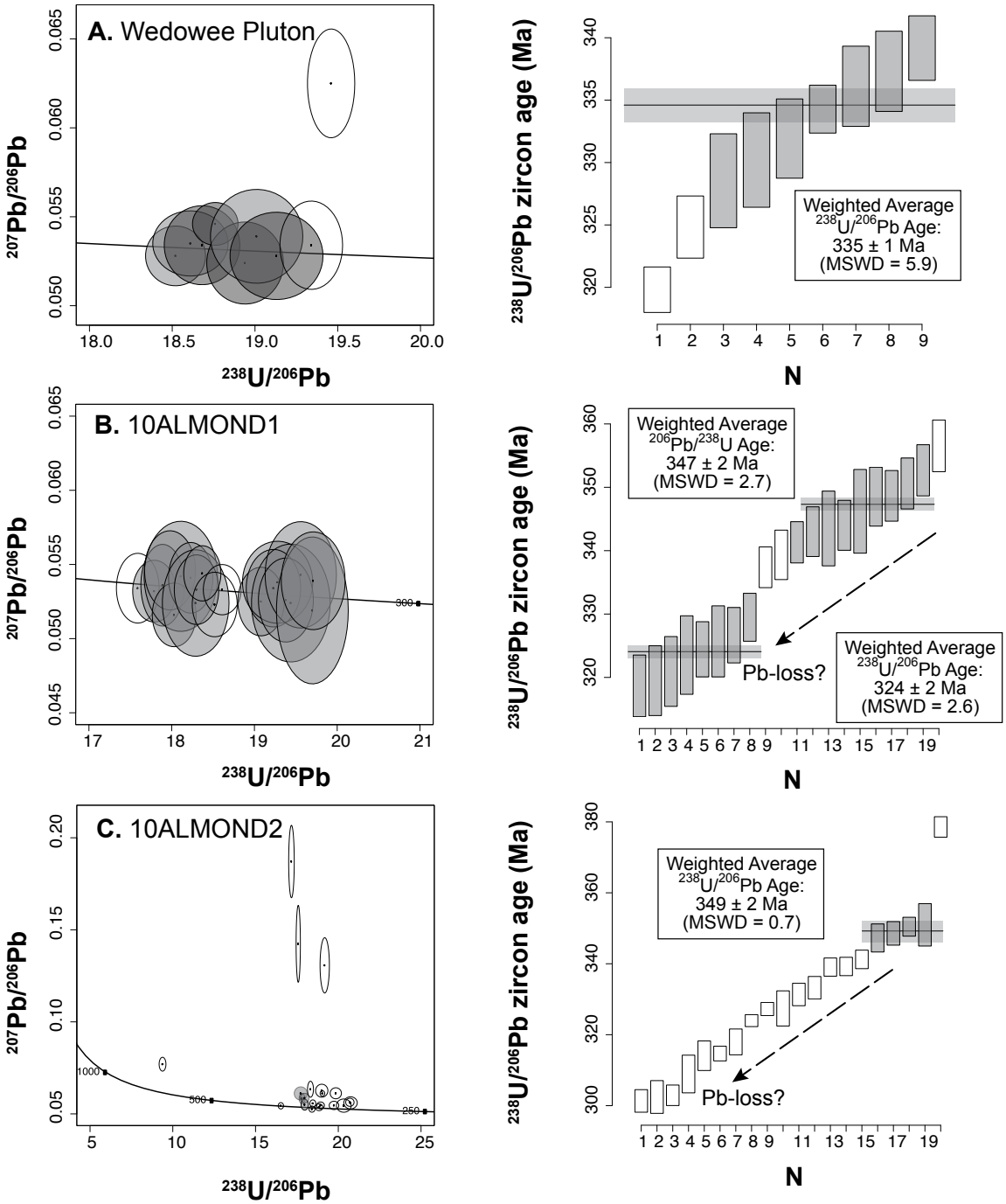

Figure 8. Tera-Wasserburg concordia plots and error-weighted average age plots for zircon in the early Alleghanian (ca. 349–335 Ma) high-Sr/Y plutons in the eastern Blue Ridge. (A) Wedowee Pluton (top). (B) Sample 10ALMOND1 (middle). (C) Sample 10ALMOND2 (bottom). All U-Pb data are plotted with 2σ uncertainties, and all calculated ages are listed as ±2σ. Ages used to calculate the weighted means are shown as gray ellipses on the Tera-Wasserburg concordia plots. U and Pb isotope data can be found in Table 5. MSWD—mean square of weighted deviates.

by complex zoning. The thickest rims were chosen for analysis, and this technique was employed with moderate success. Many analyses included multiple growth zones and/or cores. Two cores gave Grenville ages of 1.00 and 1.08 Ga. Rim $^{206}Pb/^{238}U$ dates ranged from 353 to 326 Ma, and the grains that were depth profiled from the indium mount displayed similar results. No coherent age could be found from these data (Table 5; Fig. 9A). Monazite from the Blakes Ferry Pluton occurs as euhedral to subhedral yellow crystals with an equant, prismatic morphology. Backscattered electron images revealed that the crystals have simple internal structure (Fig. DR1). The 12 grains chosen for analysis yielded an error-weighted average $^{206}Pb/^{238}U$ age of 348 ± 3 Ma (MSWD = 2). These $^{206}Pb/^{238}U$ ages for euhedral (Fig. DR2) monazite crystals (Table 5; Fig. 9B) are similar to the oldest zircon age population (346 ± 1 Ma, MSWD = 2.9); therefore, these zircons and the monazite are interpreted as the age of crystallization (Fig. 9C).

Zircon Lu-Hf Isotope Results

In both the low- and high-Sr/Y suites, intrasample initial epsilon Hf ($\varepsilon_{Hf[i]}$) values were highly variable, displaying a broad range trending from weakly positive values (up to +6) to strongly negative values (−12). We show these data as a series of probability density plots (Fig. 10) in order to illustrate the isotopic variation we observed. Only data for the Wedowee plutons display a statistically coherent population that centers at ~+2 to +3. All individual analyses give values well below Carboniferous depleted mantle values of ~+14 (Vervoort and Blichert-Toft, 1999).

DISCUSSION

Interpretation of U-Pb Ages from Plutons

The zircon U-Pb ages for all of the eastern Blue Ridge plutons are overdispersed, with MSWD values for all ages in individual samples that range from 0.7 to >>5.0. This variability may result from Pb loss from some of the zircon, ion beam sample spots that included more than one age zone in a zircon grain, and/or distinct age populations of zircon. The reconnaissance nature of the data in this study, which sampled ≤20 zircon grains per sample, cannot distinguish between these alternatives with complete certainty. However, we draw some inferences based on

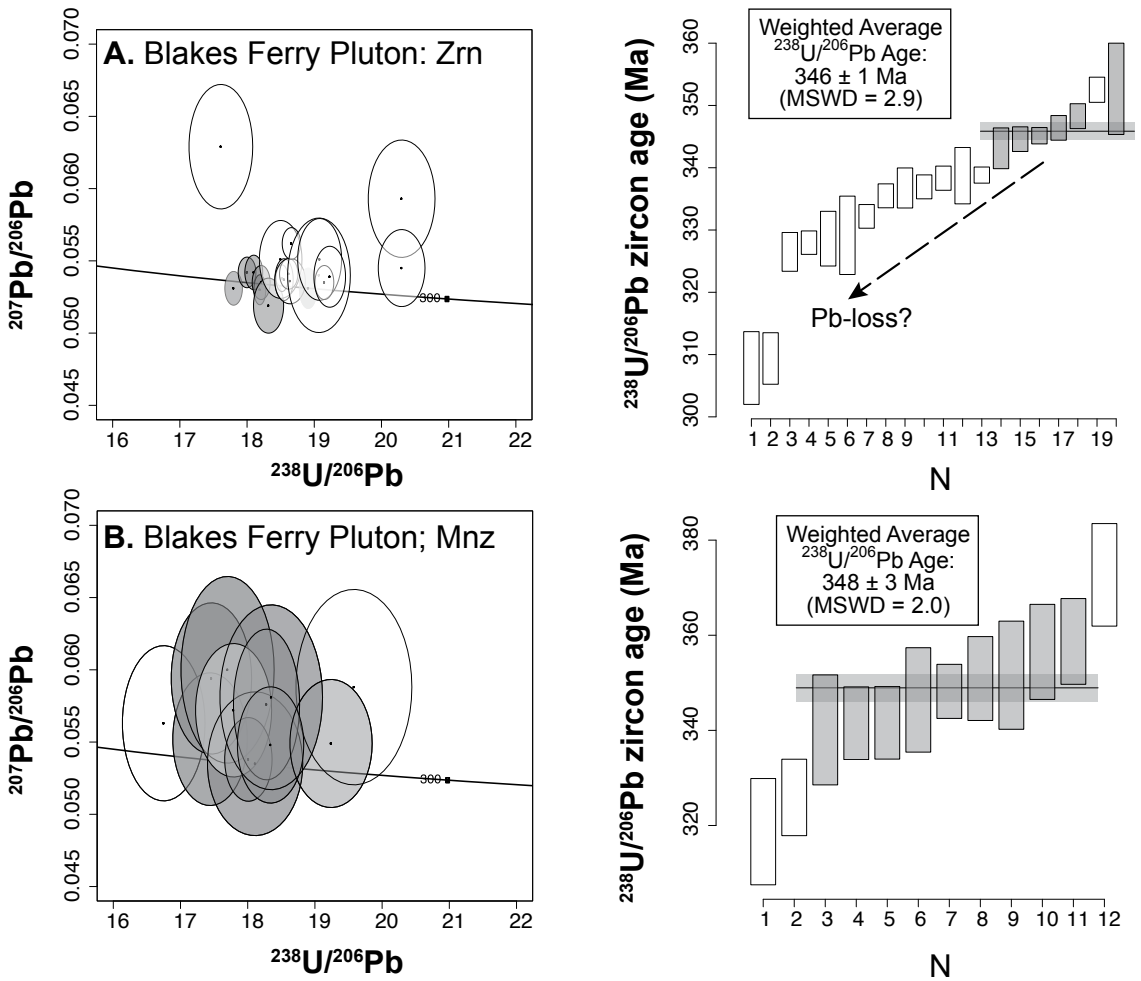

Figure 9. Tera-Wasserburg concordia plots and error-weighted average plots for the early Alleghanian (ca. 347 Ma) high-Sr/Y Blakes Ferry Pluton. (A) Blakes Ferry Pluton zircon (Zrn). (B) Blakes Ferry Pluton monazite (Mnz). All U-Pb data are plotted with 2σ uncertainties, and all calculated ages are listed as ±2σ. Ages used to calculate the weighted means are shown as gray ellipses on the Tera-Wasserburg concordia plots. U and Pb isotope data can be found in Table 5. MSWD—mean square of weighted deviates.

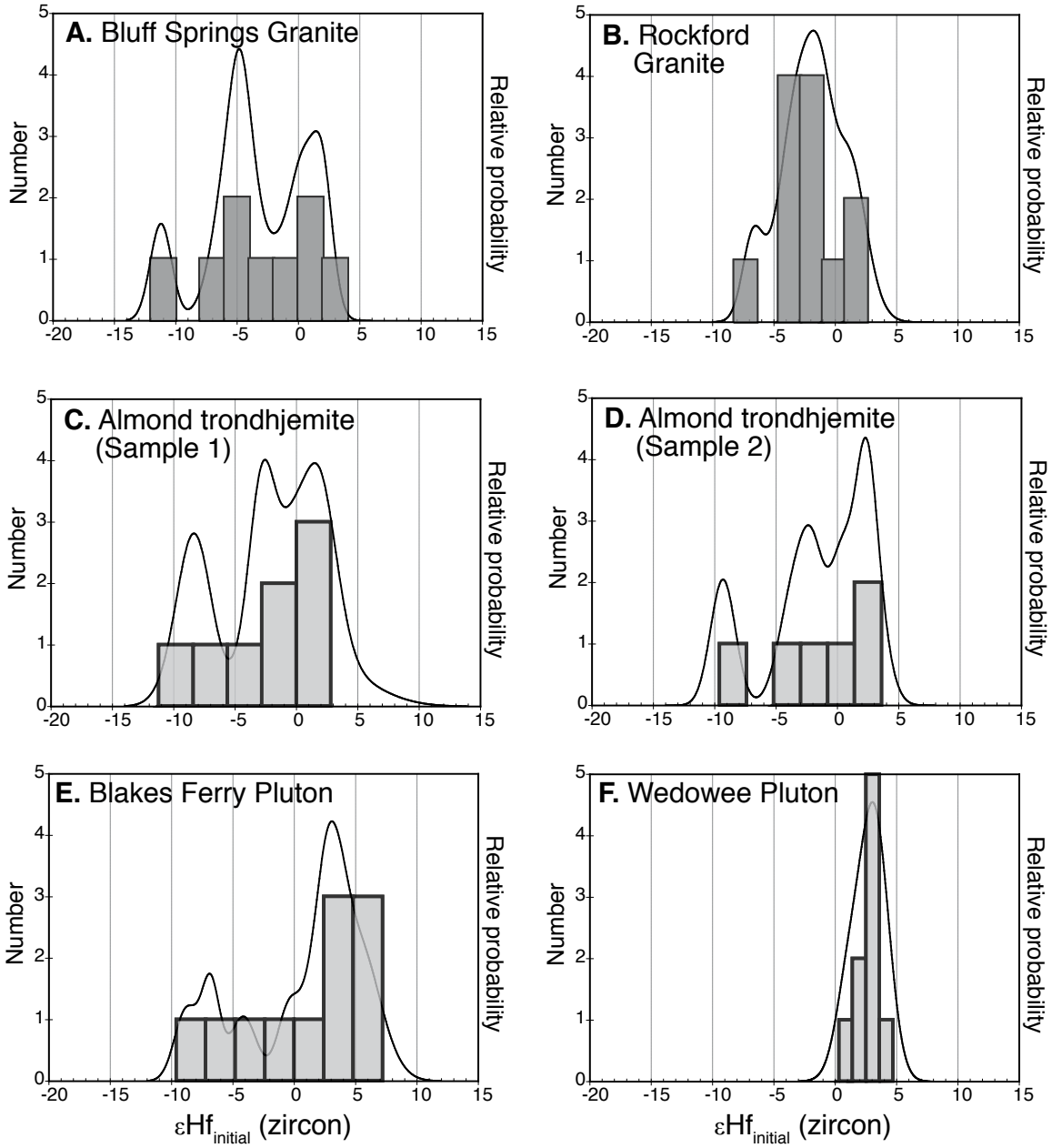

Figure 10. Relative probability plots of initial epsilon Hf ($\varepsilon_{Hf(i)}$) for plutons in the eastern Blue Ridge, Alabama. Lu and Hf isotope data can be found in Table 6.

zircon morphology and sampling, the timing of metamorphism, and age groups within the samples.

The zircon U-Pb ages from Bluff Springs Granite included two ages that are distinctly lower than the cluster of six ages at ca. 365 Ma (Fig. 7). The two younger ages at ca. 358 Ma are tentatively attributed to minor Pb loss during metamorphism between 331 and 320 Ma. Zircon U-Pb ages from the Rockford Granite form two distinct populations with no indication of stair-stepping ages between these groups (Fig. 7). We interpret both the 390 and 377 Ma age populations as igneous, based on the euhedral zircon grains and spot sampling of pyramidal crystal tips and lack of known metamorphism at 377 Ma. The Rockford Granite may be composite, with more than one magmatic episode, and we infer that the zircons forming the older age group were inherited from an early pulse of magma. Zircon U-Pb ages from the Wedowee Pluton included two discordant grains that likely lost Pb. The remaining six analyses form a stair-step array from ca. 339 to 329 Ma (Fig. 8). Although these analyses are concordant within uncertainty, the range of ages is inferred to result from limited Pb loss during metamorphism. The youngest zircon ages match the garnet Sm-Nd age at ca. 331 Ma, supporting this interpretation. Zircon U-Pb ages from the Almond trondhjemites also form stair-step arrays (Fig. 8), which extend from ca. 351 to 284 Ma (Fig. 8; Table 5), excluding ages of 652 and 641 Ma, which are interpreted as inherited. The zircon U-Pb ages obtained from depth profiling (Table 5) are similar in range to those obtained from spots on sections through the crystals

and are included in the plots. However, the ages from depth profiling include the oldest and youngest ages for this sample. Four of the oldest analyses from depth profiling Almond2 zircon yielded an error-weighted average $^{206}Pb/^{238}U$ age of 349 ± 2 Ma, MSWD = 0.7 (Fig. 8C). Unlike the Wedowee Pluton ages, the majority of data from Almond1 form two groups at ca. 347 and ca. 324 Ma. Based on ages and uncertainties, we infer that intrusion was between 351 and 345 Ma. Almond2 analyses show extensive discordance (Fig. 8), likely from Pb loss. Therefore, we interpret that the range of zircon ages toward younger values is, at least in part, a result of Pb loss during metamorphism, which garnet Sm-Nd ages establish as between 331 and 320 Ma. Zircon U-Pb ages from the Blakes Ferry Pluton have the greatest range of the pluton ages presented here: ca. 360–310 Ma (Fig. 9). Like the Almond U-Pb data, the Blakes Ferry zircon data include numerous discordant analyses. Therefore, the large range in age is interpreted to result from metamorphic Pb loss, which resulted in ages ranging down to Alleghanian. The weighted mean age of 346 ± 1 Ma (MSWD = 2.9) for five of the six oldest zircon matches well with the U-Pb ages for the euhedral monazite grains at ca. 348 Ma, and we interpret igneous crystallization at ca. 347 Ma.

Timing and Significance of Paired Magmatic Belt Construction

The magmatic evolution of paired high- and low-Sr/Y magmatic belts in collisional orogenic belts commonly follows a temporal pattern involving (1) early, low-Sr/Y magmatism, often characterized by calc-alkaline, basalt-andesite-dacite-rhyolite associations, followed by (2) contractional deformation involving collision of buoyant tectonic plates, and finally (3) late- to postkinematic, high-Sr/Y magmatism (cf. Tulloch and Kimbrough, 2003; Chung et al., 2009; Schwartz et al., 2011). In the Tibetan Himalayas, this temporal pattern occurred over >100 m.y. and involved calc-alkaline, low-Sr/Y magmatism from 140 to 40 Ma, followed by collision at ca. 60–50 Ma, and postkinematic high-Sr/Y magmatism at 40–10 Ma (Chung et al., 2005; Xu et al., 2010; Zeng et al., 2011). Both low- and high-Sr/Y magmatic belts overlap spatially, but they are geochemically and temporally distinct—features that we also observe in Alabama.

In the Alabama sector of the eastern Blue Ridge, paired magmatic belts also formed during convergent margin orogenesis. U-Pb zircon age determinations from low- and high-Sr/Y plutonic rocks suggest that these belts were temporally distinct, with peak magmatic activity in the low-Sr/Y suite ranging from ca. 390 to 365 Ma, whereas magmatism in the high-Sr/Y plutons ranged from ca. 349 to 335 Ma. These results are intriguing because they imply (1) a restricted period of low-Sr/Y magmatism that preceded high-Sr/Y magmatism, (2) early, Neoacadian deformation and magmatism in the low-Sr/Y belt that preceded high-Sr/Y magmatism, (3) a possible magmatic gap between the paired belts, and (4) postmagmatic peak metamorphism, and loading of the crust immediately following high-Sr/Y magmatism. Our ages for the low- and high-Sr/Y magmatic belt overlap with those along strike of the orogen (e.g., eastern Blue Ridge—Miller et al., 2000; B.V. Miller et al., 2006; Inner Piedmont—Mapes, 2002; Giorgis et al., 2002), suggesting that paired magmatic belts extend over the entire length of the Southern Appalachians for more than 600 km.

The temporal transition from low- to high-Sr/Y magmatism signifies an important change in magma generation processes that we hypothesize was related to changes in crustal thickness in the Alabama eastern Blue Ridge. Importantly, these two overlapping belts occur within the eastern Blue Ridge and are not separated by major faults (e.g., Brevard fault zone), as observed in Georgia and North Carolina, thereby limiting uncertainties associated with younger fault displacements. Geochemical models for the trondhjemite and granodiorite magmas in the eastern Blue Ridge of Georgia and North Carolina are consistent with intracrustal partial melting involving amphibole and biotite dehydration reactions, leaving behind a plagioclase-poor, garnet-bearing residue at deep-crustal levels (>30 km depth; Miller et al., 1997). Highly variable and negative zircon Hf isotope data from the Alabama plutons support an intracrustal melting origin; however, some weakly positive $\varepsilon_{Hf(i)}$ values are compatible with contributions from a mantle source. A more precise evaluation of the source region for these magmas requires additional isotopic information (e.g., zircon oxygen isotopes) to evaluate possible mantle contributions.

Heat sources for the early Alleghanian metamorphism, which is less widespread to the northeast along strike, are not well understood. In orogenic belts, various mechanisms are commonly invoked to explain thermal perturbations. For example, heat-producing processes may include: (1) intracrustal radioactive self-heating; (2) crustal thickening and thermal relaxation of isotherms; and (3) advection of heat by partially melted underlying mantle, which could result from flux melting of the mantle wedge, slab break-off, and/or lithospheric delamination. In the case of the Tibetan Himalaya, where high- and low-Sr/Y plutons are also observed, previous workers have documented depleted mantle isotopic signatures in high-Sr/Y plutons, suggesting the involvement of mantle sources in their generation (e.g., Xu et al., 2010). This result raises the question of how mantle sources may contribute to the origin of syn- to late-kinematic high-Sr/Y magmatic belts in collisional orogens.

The controversial role of crustal versus mantle melting during orogenesis has led to a variety of models for the magmatism and the tectonic evolution of the Southern Appalachians. Green et al. (2015) interpreted the Elkahatchee Quartz Diorite and Hog Mountain Pluton as derived from crustal igneous rocks. However, most authors agree that Neoacadian, low-Sr/Y plutons were generated by intracrustal partial melting of supracrustal rocks (e.g., Drummond et al., 1997; Giorgis et al., 2002). The origin of high-Sr/Y plutons is more controversial. For example, previous authors have argued that they may have originated from (1) partial melting of subducted oceanic crust (Defant et al., 1988), and/or (2) intracrustal melting (Sinha, et al., 1989; Miller et al., 1997; B.V. Miller et al., 2006). The role of mantle melting has received little attention in the Neoacadian orogen; however, slab break-off and delamination have been proposed for the younger Alleghanian orogen from 320 to 300 Ma (Sacks and Secor, 1990; Nelson, 1992; Samson et al., 1995). Our new $\varepsilon_{Hf(i)}$ data for zircon in both the low- and high-Sr/Y plutons indicate a crustal signature with possible mantle contributions for Neoacadian to early Alleghanian magmas. The high-Sr/Y Wedowee Pluton is the only eastern Blue Ridge pluton that has a narrow range of positive initial Hf values in zircon ($\varepsilon_{Hf[i]}$ = 0 to +5), compatible with a mantle source. These data, combined with the high-Sr/Y ratios, are compatible with a lower-crustal source region containing garnet, or mixing between crustal and mantle melts.

We follow previous workers in hypothesizing that low-Sr/Y plutons were generated by midcrustal partial melting of existing continental crust, and we propose that high-Sr/Y magmas were generated from deep-crustal or lithospheric partial melting (>30 km depth) of arc lithosphere, leaving behind a garnet amphibolite residue. We propose that advection of mantle heat and basaltic underplating at the base of the crust drove deep-crustal melting from 350 to 335 Ma. We suggest that advection of mantle heat to the lower crust created a "hot zone," where mantle-derived mafic melts mingled and induced dehydration partial melting of Grenville-age crust. This resulted in the generation of high-Sr/Y magmatism with mixed negative to positive $\varepsilon_{Hf(i)}$ zircon values. We speculate that the source of the mantle contribution may have involved delamination of the lower crust/lithosphere and/or transtensional upwelling of asthenospheric mantle.

Crustal Thickness during the Neoacadian–Alleghanian Orogenies

Rocks currently exposed at the surface must have been subject to a load corresponding to the estimated metamorphic pressure. Depths calculated from metamorphic pressure estimates provide a minimum crustal thickness, because the crust at that time likely extended below the depth calculated for the samples. Rocks below the samples and above the master detachment fault are inferred to have been part of the pre-Alleghanian thrusting continental crust, and not mantle, based on the seismic velocities determined in Georgia during the COCORP experiment (Cook et al., 1979; Nelson et al., 1985, 1987; McBride and Nelson, 1991). The present depth to the master detachment in the Blue Ridge of Alabama is established as ~6 km, based on well and seismic reflection data (e.g., Thomas, 2004). Ignoring thickening within the thrust sheet that might have occurred after metamorphism, the crustal section above the detachment, combined with estimates based on metamorphic pressures, indicates crustal thicknesses of at least 27–39 km for Neoacadian crust for the Wedowee and Josie Leg rocks, respectively. The master detachment is within sedimentary rocks and is underlain by autochthonous crystalline Grenville basement (e.g., Thomas, 2004; Steltenpohl, 2005; McClellan et al., 2007; Tull et al., 2007); therefore, if the Wedowee and Emuckfaw rocks are of North American affinity, it is reasonable to assume that they were deposited on Grenville basement. These basement rocks would likely add considerably more to the total crustal thickness during the Alleghanian; however, because the eastern Blue Ridge was likely transported >120 km to the northwest during the Alleghanian (e.g., Cook et al., 1979; Thomas, 2004, 2011), this section of Grenville crust and its thickness are unknown. Therefore, the 27–39 km crustal thickness estimates are minima for ca. 330–320 Ma.

Tectonic Interpretations

The ε_{Nd} estimates for the Wedowee Group and Emuckfaw Group rocks indicate that detritus was derived from continental crustal rocks and that little or no juvenile material was incorporated at the three locations that were sampled. Clearly, additional data targeted to span the stratigraphic section are needed. However, the small Nd isotope data set presented here provides no evidence for juvenile rocks sourcing sedimentation, which was likely occurred ca. 450 Ma. The large percent of Grenville-age zircon grains in the Wedowee and Emuckfaw Groups (Barineau et al., 2015) and the Nd isotope results are compatible with a source region that was restricted to Laurentian basement and possibly overlying sediments. These results seem at odds with the interpretation by Barineau et al. (2015) that the Wedowee and Emuckfaw Groups were deposited in a back-arc setting, which would likely have received isotopically juvenile detritus from the nearby magmatic arc.

The new ages that we present here indicate that the peak of metamorphism in the eastern Blue Ridge occurred prior to or during the initial Carboniferous deposition of orogenic detritus in the Black Warrior Basin in northwestern Alabama. The new garnet Sm-Nd ages and *P-T* estimates for the eastern Blue Ridge rocks require that peak metamorphism and crustal thickening occurred from 331 to 320 Ma. Therefore, the oldest garnet growth was synchronous with deposition of the Mississippian Bangor Limestone in the Black Warrior Basin of Alabama (e.g., Pashin, 1994). This garnet growth may have initiated prior to much of the displacement along the master fault beneath the Blue Ridge thrust sheet, because significant detrital input into the Black Warrior Basin is not recognized in rocks below the Pottsville Formation (Pashin, 1994; Pashin and Gastaldo, 2009). The youngest garnet dated here, ca. 320 Ma, grew synchronous with the initial deposition of the siliciclastic Parkwood Formation (Fig. 11) and is statistically indistinguishable from the lowermost Pottsville Formation

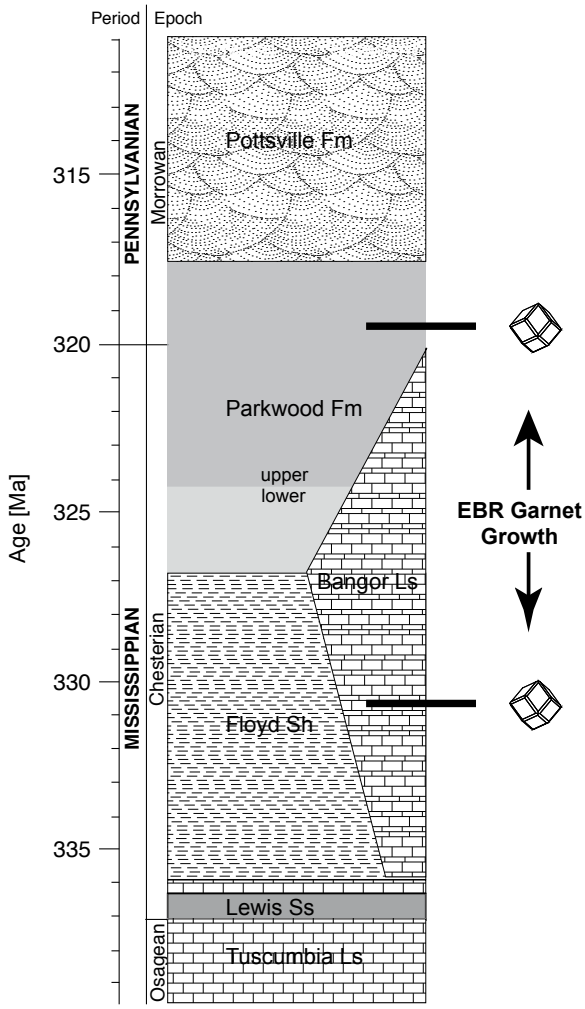

Figure 11. Stratigraphic column of Upper Mississippian to Lower Pennsylvanian rocks in the Black Warrior Basin showing the timing of metamorphic garnet growth in the eastern Blue Ridge (EBR), modified from Pashin and Gastaldo (2009). Ls—Limestone; Ss—Sandstone; Sh—Shale.

at 317.5 Ma (Pashin and Gastaldo, 2009). These garnets grew in rocks that peaked at staurolite zone metamorphic conditions, and some of the garnet contains staurolite inclusions. Thus, the Alleghanian metamorphic peak in the eastern Blue Ridge occurred during initial sedimentation in the foreland basin, which rests on Laurentian basement.

Metamorphic rocks southeast of the Towaliga and Goat Rock faults cooled through the closure temperature for Ar in hornblende at ca. 295–288 Ma (Steltenpohl et al., 2008). In addition, post-tectonic granitoids intruded on both sides of the Suwannee suture between 330 and 300 Ma (Ma et al., 2012). These plutons are interpreted to result from crustal anatexis and not suprasubduction-zone magmatism. Therefore, it is possible that the Alleghanian orogen was >~100 km wide (present-day width) and more complex than previously realized. Although rocks of the Uchee terrane could have been heated at ca. 320 Ma, alternatively, the Uchee metamorphic peak may have been later than that in the eastern Blue Ridge, ca. 300 Ma. Little is known about the timing of Inner Piedmont metamorphism between these locations because peak metamorphic ages younger than 400 Ma are not widely reported. The Alleghanian thrust sheet from

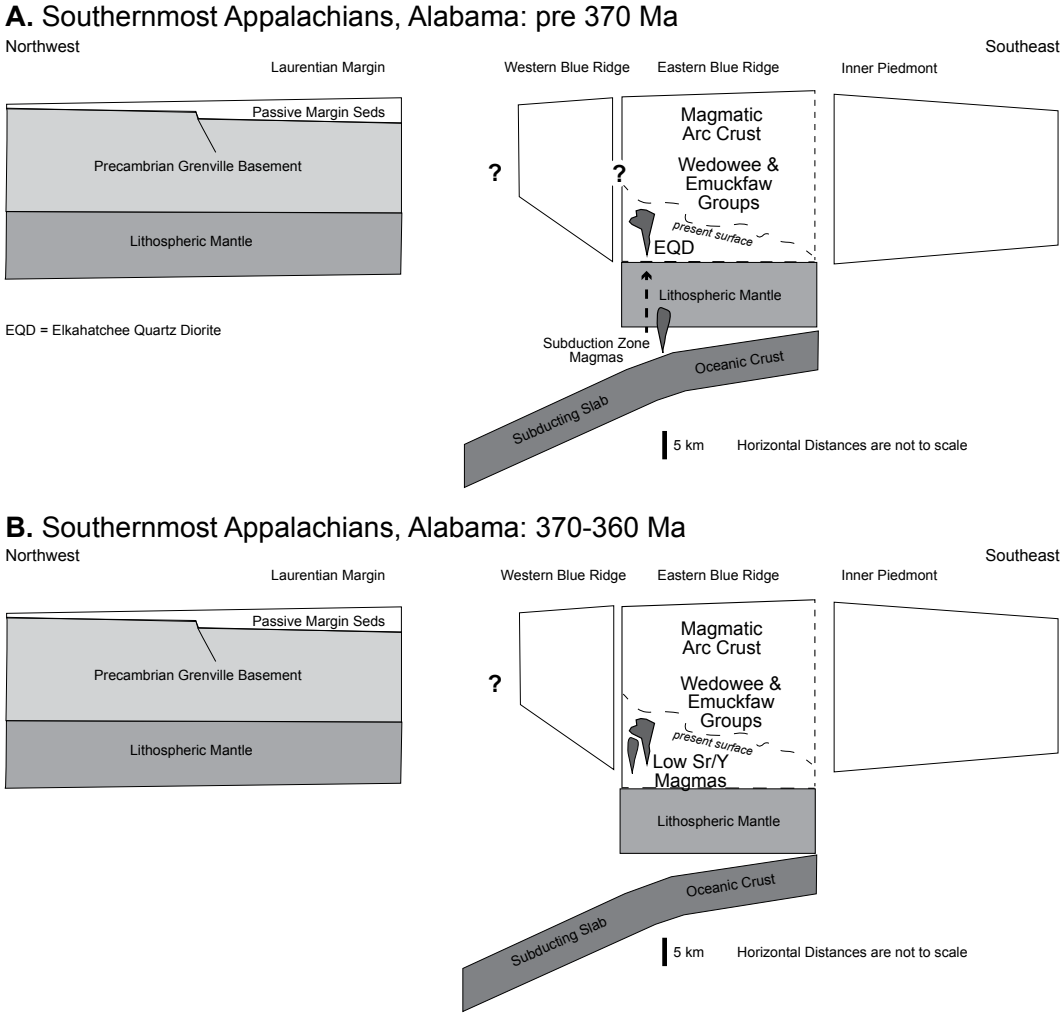

Figure 12. Cartoons showing the Laurentian margin, eastern Blue Ridge, and the inferred subducting slab beneath the Alabama Blue Ridge. (A) Laurentian margin and outboard magmatic arc prior to 370 Ma. The earliest eastern Blue Ridge plutons, e.g., the earliest Elkahatchee rocks and Hog Mountain Pluton, intruded the arc at this time. (B) Laurentian margin and outboard magmatic arc between 370 and 360 Ma. The low-Sr/Y Rockford and Bluff Springs plutons, which are interpreted as intracrustal melts, intruded during this period. This melting is inferred to reflect thickened crust at this time. (C) Laurentian margin and outboard magmatic arc between ca. 330 and 320 Ma. The high-Sr/Y Wedowee, Almond, and Blakes Ferry plutons intruded shortly prior to or during this time interval. Garnet growth in the Wedowee (WGrt) and Emuckfaw (EGrt) Groups is shown at the depths required for estimated metamorphic pressures. All of the crustal thicknesses in the eastern Blue Ridge are shown as minimums for the metamorphic pressure estimates; however, 6 km of crust is added beneath the Emuckfaw sample in order to include rocks currently between the Josie Leg sample and Appalachian master décollement. Seds—sediments.

the eastern Blue Ridge to the Uchee terrane could have a diachronous thermal structure resulting from progressive cooling and exhumation as hot midcrustal rocks moved up and over the Laurentian margin on the master décollement. Alternatively, there may have been more than one hot orogenic core between 330 and 280 Ma.

Previous publications have proposed that the Inner Piedmont includes the core of a Taconic magmatic arc that was constructed above a NW-dipping subduction zone (e.g., Hatcher, 2010). The eastern Blue Ridge rocks have been interpreted as an Ordovician back-arc basin built upon the Laurentian margin (Tull et al., 2014; Barineau et al., 2015). NW-dipping subduction beneath an outboard island arc most likely began during the Late Ordovician (e.g., Hatcher, 2010). In Alabama, evidence for arc magmatism includes the ca. 441 Ma Kowaliga Gneiss (Grimes et al., 1997), the ca. 440 Ma Farmville Metagranite (Hawkins et al., 2013), and the 450–440 Ma Dadeville Complex (Tull et al., 2018). The Late Ordovician magmatic arc may not have developed on the Laurentian margin and instead may have been offshore or separated from the continent by a back-arc basin (Tull et al., 2014; Barineau et al., 2015). The ages and metamorphic data presented here indicate that the Ordovician arc magmatism likely did not extend northwest into what is currently the eastern Blue Ridge, and that the metasedimentary rocks in the Blue Ridge were not heated (and loaded) until near the end of the Neoacadian orogeny. However, the petrological and geochronological data from the earliest plutons (Elkahatchee Quartz Diorite and Hog Mountain Pluton) are compatible with subduction beneath the eastern Blue Ridge during the Neoacadian. Although the subduction setting is not well known, we postulate that oceanic or back-arc crust was subducted beneath the Laurentian margin at ca. 380 Ma (Fig. 12). Ages for low-Sr/Y magmatism (390–365 Ma), high-Sr/Y magmatism at 345–335 Ma, garnet growth from 331 to 320 Ma, and loading during garnet growth indicate that the crust thickened during the earliest Alleghanian (Figs. 12B and 12C).

CONCLUSIONS

The geochemical characteristics of 390–335 Ma (Neoacadian to early Alleghanian) plutons in the eastern Blue Ridge of Alabama track changes from possibly subduction-related melts that produced tonalite and granodiorite plutons ca. 390–370 Ma (e.g., Hog Mountain Pluton), through low-Sr/Y intracrustal melts ca. 390–365 Ma (e.g., Rockford and Bluff Springs Granites), to high-Sr/Y melts ca. 349–335 Ma (e.g., Almond, Wedowee, and Blakes Ferry Plutons) that had a deep-crustal source. The high Sr/Y melts include possible mantle input and could reflect mantle upwelling.

Garnet Sm-Nd ages for amphibolite-facies metamorphism of pelitic rocks in the Wedowee and Emuckfaw Groups surrounding these plutons indicate that metamorphism occurred during the earliest Alleghanian, between 331 and 320 Ma. There is no evidence for pre–330 Ma metamorphism in the garnet. The extensive early Alleghanian garnet zone metamorphism documented in the Alabama Blue Ridge differs considerably from the Blue Ridge in North Carolina, where Alleghanian metamorphic temperatures have been interpreted as ≤350 °C (e.g., Miller et al., 2006). Modest pressure increases inferred from garnet compositional zoning and isochemical phase diagram sections indicate that crustal thickening was approximately synchronous with high-Sr/Y magmatism in the eastern Blue Ridge.

Initial garnet growth in the eastern Blue Ridge was synchronous with deposition of carbonate sediments in the Appalachian foreland basin on the Laurentian margin (Floyd Shale and Bangor Limestone). The last garnet growth in the eastern Blue Ridge was simultaneous with deposition of clastic sediments in the foreland basin (Parkwood Formation and lowermost Pottsville Formation of the Black Warrior Basin; Pashin, 1994; Pashin and Gastaldo, 2009). The Floyd Shale was interpreted by Pashin and Gastaldo (2009) as accumulating prior to the Alleghanian orogeny; however, the new ages for garnet growth from the Wedowee and Emuckfaw Groups indicate orogenesis ca. 330 Ma. This synchronicity of metamorphism and deposition is compatible with initial exhumation of a metamorphic core during the peak of metamorphism. The 330–320 Ma orogenic core indicates that the Alleghanian orogeny began significantly earlier than 318 Ma, as indicated in Pashin and Gastaldo (2009), or that precollisional metamorphism occurred in a magmatic arc seaward of the Laurentian margin. We conclude that the combination of metamorphic, igneous, and sedimentary data with a robust geochronological data set is a powerful means for reconstructing crustal history.

ACKNOWLEDGMENTS

This work was made possible with financial support from the University of Alabama Department of Geological Sciences Advisory Board, Hooks Fund, and Graduate School Research and Travel Support Fund. Drew Coleman at the University of North Carolina at Chapel Hill provided assistance with Sm-Nd isotope data collection. Rob Holler and Ian Anderson provided assistance with electron microprobe analysis at the University of Alabama. Crystal Hout and Karen Parker provided valuable assistance with Sm and Nd sample analysis. Joe Wooden and Matt Coble provided assistance with U-Pb isotope data collection on the sensitive high-resolution ion microprobe–reverse geometry (SHRIMP-RG) at Stanford. We thank Kurt Stuewe for helpful comments and efficient editorial handling. Three anonymous *Lithosphere* reviewers provided thorough reviews and very helpful comments.

REFERENCES CITED

Barineau, C.I., Tull, J.F., and Holm-Denoma, C.S., 2015, A Laurentian margin back-arc: The Ordovician Wedowee-Emuckfaw-Dahlonega basin, *in* Holmes, A.E., ed., Diverse Excursions in the Southeast: Paleozoic to Present: Geological Society of America Field Guide 39, p. 21–78, https://doi.org/10.1130/2015.0039(02).

Bhattacharya, A., Mohanty, L., Maji, A., Sen, S.K., and Raith, M., 1992, Non-ideal mixing in the phlogopite-annite boundary: Constraints from experimental data on Mg-Fe partitioning and a reformulation of the biotite-garnet geothermometer: Contributions to Mineralogy and Petrology, v. 111, p. 87–93, https://doi.org/10.1007/BF00296580.

Carlson, W., 2006, Rates of Fe, Mg, Mn, and Ca diffusion in garnet: The American Mineralogist, v. 91, p. 1–11, https://doi.org/10.2138/am.2006.2043.

Carlson, W., 2012, Rates and mechanism of Y, REE, and Cr diffusion in garnet: The American Mineralogist, v. 97, p. 1598–1618, https://doi.org/10.2138/am.2012.4108.

Chung, S.L., Chu, M.-F., Zhang, Y., Xie, Y., Lo, C.-H., Lee, T.-Y., and Lan, C.-Y., 2005, Tibetan tectonic evolution inferred from spatial and temporal variations in post-collisional magmatism: Earth-Science Reviews, v. 68, no. 3–4, p. 173–196, https://doi.org/10.1016/j.earscirev.2004.05.001.

Chung, S.L., Chu, M.F., Ji, J., O'Reilly, S.Y., Pearson, N.J., Lui, D., Lee, T.Y., and Lo, C.H., 2009, The nature and timing of crustal thickening in southern Tibet: Geochemical and zircon Hf isotopic constraints from postcollisional adakites: Tectonophysics, v. 477, no. 1–2, p. 36–48, https://doi.org/10.1016/j.tecto.2009.08.008.

Cook, F., Albaugh, D., Brown, L., Kaufman, S., Oliver, J., and Hatcher, R.D., Jr., 1979, Thin-skinned tectonics in the crystalline Southern Appalachians: COCORP seismic profiling of the Blue Ridge and Piedmont: Geology, v. 7, p. 563–567, https://doi.org/10.1130/0091-7613(1979)7<563:TTITCS>2.0.CO;2.

de Capitani, C., and Brown, T.H., 1987, The computation of chemical equilibrium in complex systems containing nonideal solutions: Geochimica et Cosmochimica Acta, v. 51, p. 2639–2652, https://doi.org/10.1016/0016-7037(87)90145-1.

de Capitani, C., and Petrakakis, K., 2010, The computation of equilibrium assemblage diagrams with Theriak/Domino software: The American Mineralogist, v. 95, p. 1006–1016, https://doi.org/10.2138/am.2010.3354.

Defant, M.J., Drummond, M.S., Arthur, J.D., and Ragland, P.C., 1988, An example of trondhjemite petrogenesis: The Blakes Ferry pluton, Alabama, U.S.A.: Lithos, v. 21, p. 161–181, https://doi.org/10.1016/0024-4937(88)90007-2.

Donovan, J., 2010, Probe for EPMA: Eugene, Oregon, Probe Software, https://www.probesoftware.com/index.html (accessed June 2019).

Drummond, M.S., and Allison, D.T., 1987, Rockford Granite, Coosa County, Alabama: III. Igneous petrogenesis and tectonic setting, *in* Drummond, M.S., and Green, N.L., eds., Granites of Alabama: Tuscaloosa, Alabama, Geological Survey of Alabama, Special Publication, p. 117–130.

Drummond, M.S., Wesolowski, D., and Allison, D.T., 1988, Generation, diversification, and emplacement of the Rockford Granite, Alabama Appalachians: Mineralogic, petrologic, isotopic (C & O), and *P-T* constraints: Journal of Petrology, v. 29, p. 869–897, https://doi.org/10.1093/petrology/29.4.869.

Drummond, M.S., Defant, M.J., and Kepezhinskas, P.K., 1996, Petrogenesis of slab-derived trondhjemite-tonalite-dacite/adakite magmas: Transactions of the Royal Society of Edinburgh–Earth Sciences, v. 87, p. 205–215, https://doi.org/10.1017/S0263593300006611.

Drummond, M.S., Neilson, M.J., Allison, D.T., and Tull, J.F., 1997, Igneous petrogenesis and tectonic setting of granitic rocks from the eastern Blue Ridge and Inner Piedmont, Alabama Appalachians, *in* Sinha, A.K., Whalen, J.B., and Hogan, J.P., eds., The Nature of

Magmatism in the Appalachian Orogen: Geological Society of America Memoir 191, p. 147–164, https://doi.org/10.1130/0-8137-1191-6.147.

Eddy, M.P., Ibañez-Mejia, M., Burgess, S.D., Coble, M.A., Cordani, U.G., DesOrmeau, J., Gehrels, G.E., Li, X., MacLennan, S., Pecha, M., Sato, K., Schoene, B., Valencia, V.A., Vervoort, J.D., and Wang, T., 2019, GHR1 zircon—A new Eocene natural reference material for microbeam U-Pb geochronology and Hf isotopic analysis of zircon: Geostandards and Geoanalytical Research, v. 43, p. 113–132, https://doi.org/10.1111/ggr.12246.

Gastaldo, R.A., Guthrie, G.M., and Steltenpohl, M.G., 1993, Mississippian fossils from Southern Appalachian metamorphic rocks and their implications for late Paleozoic tectonic evolution: Science, v. 262, p. 732–734, https://doi.org/10.1126/science.262.5134.732.

Gatewood, M.P., and Stowell, H.H., 2017, Thrust loading as a mechanism for crustal recycling: An example from the Swakane Gneiss, Cascades crystalline core, Washington, USA, *in* Law, R.D., Thigpen, J.R., Merschat, A.J., and Stowell, H.H., eds., Linkages and Feedbacks in Orogenic Systems: Geological Society of America Memoir 213, p. 255–278, https://doi.org/10.1130/2017.1213(11).

Gibson, R.G., and Speer, J.A., 1986, Contact aureoles as constraints on regional *P-T* trajectories: An example from the northern Alabama Piedmont, USA: Journal of Metamorphic Geology, v. 4, p. 285–308, https://doi.org/10.1111/j.1525-1314.1986.tb00352.x.

Giorgis, S.D., Mapes, R.W., and Bream, B.R., 2002, The Walker Top Granite: Acadian granitoid or eastern Inner Piedmont basement?, *in* Hatcher, R.D., Jr., and Bream, B.R., eds., Inner Piedmont Geology in the South Mountains–Blue Ridge Foothills and the Southwestern Brushy Mountains, Central-Western North Carolina: Raleigh, North Carolina Geological Survey, Carolina Geological Society Guidebook, p. 33–43.

Green, N.L., Stowell, H.H., Bersch, M.G., Lesher, C.M., and Sinha, A.K., 2015, Cumulus-intercumulus liquid mixing in the Hog Mountain Pluton, southern Appalachian orogen, *in* Stowell, H., Odom Parker, K., and Madden, J., eds., Neoacadian and Alleghanian Intrusion, Metamorphism, and Gold Mineralization in the Eastern Blue Ridge: Tuscaloosa, Alabama Geological Society, Guidebook for the 52nd Annual Field Trip, p. 11–37.

Grimes, J., Heatherington, A.L., Mueller, P.A., and Steltenpohl, M.G., 1997, Tectonic implications of Ordovician U-Pb zircon dates from the Farmville metagranite: Geological Society of America Abstracts with Programs, v. 28, p. 21.

Groshong, R.H., Jr., Hawkins, W.B., Jr., Pashin, J.C., and Harry, D.L., 2010, Extensional structures of the Alabama Promontory and Black Warrior foreland basin: Styles and relationship to the Appalachian fold-thrust belt, *in* Tollo, R.P., Bartholomew, M.J., Hibbard, J.P., and Karabinos, P.M., eds., From Rodinia to Pangea: The Lithotectonic Record of the Appalachian Region: Geological Society of America Memoir 206, p. 579–605, https://doi.org/10.1130/2010.1206(23).

Hatcher, R.D., Jr., 1987, Tectonics of the Southern and Central Appalachian Internides: Annual Review of Earth and Planetary Sciences, v. 15, p. 337–362, https://doi.org/10.1146/annurev.ea.15.050187.002005.

Hatcher, R.D., Jr., 1989, Tectonic synthesis of the U.S. Appalachians, *in* Hatcher, R.D., Jr., Thomas, W.A., and Viele, G.W., eds., The Appalachian-Ouachita Orogen in the United States: Boulder, Colorado, Geological Society of America, Geology of North America, v. F-2, p. 511–535, https://doi.org/10.1130/DNAG-GNA-F2.511.

Hatcher, R.D., Jr., 2001, Rheological partitioning during multiple reactivation of the Paleozoic Brevard fault zone, Southern Appalachians, USA, *in* Holdsworth, R.E., et al., eds., The Nature and Tectonic Significance of Fault Zone Weakening: Geological Society [London] Special Publication 186, p. 257–271, https://doi.org/10.1144/GSL.SP.2001.186.01.15.

Hatcher, R.D., Jr., 2002, The Alleghanian (Appalachian) orogeny, a product of zipper tectonics: Rotational transpressive continent-continent collision and closing of ancient oceans along irregular margins, *in* Martínez Catalán, J.R., et al., eds., Variscan-Appalachian Dynamics: The Building of the Late Paleozoic Basement: Geological Society of America Special Paper 364, p. 199–208, https://doi.org/10.1130/0-8137-2364-7.199.

Hatcher, R.D., Jr., 2010, The Appalachian orogen: A brief summary, *in* Tollo, R.P., Bartholomew, M.J., Hibbard, J.P., and Karabinos, P.M., eds., From Rodinia to Pangea: The Lithotectonic Record of the Appalachian Region: Geological Society of America Memoir 206, p. 1–19.

Hatcher, R.D., Jr., and Zeitz, I., 1980, Tectonic implications of regional aeromagnetic and gravity data from the southern Appalachians, *in* Wones, D., eds., Proceedings of the Caledonide Orogen Project: The Caledonides in the U.S.A.: Virginia Polytechnic Institute and State University Memoir 2, p. 235–244.

Hatcher, R.D., Jr., Bream, B.R., and Merschat, A.J., 2007, Tectonic map of the Southern and Central Appalachians: A tale of three orogens and a complete Wilson cycle, *in* Hatcher, R.D., Jr., Carlson, M.P., McBride, J.H., and Martínez Catalán, J.R., eds., 4-D Framework of Continental Crust: Geological Society of America Memoir 200, p. 211–231, https://doi.org/10.1130/2007.1200(29).

Hawkins, J.F., Steltenpohl, M.G., Zou, H., Mueller, P.A., and Schwartz, J.J., 2013, New constraints on Ordovician magmatism in the southernmost exposures of the eastern Blue Ridge in Alabama: Geological Society of America Abstracts with Programs, v. 45, no. 2, p. 62.

Hibbard, J., Stoddard, E., Secor, D., and Dennis, A., 2002, The Carolina zone: Overview of Neoproterozoic to early Paleozoic peri-Gondwanan terranes along the eastern flank of the Southern Appalachians: Earth-Science Reviews, v. 57, p. 299–339, https://doi.org/10.1016/S0012-8252(01)00079-4.

Hibbard, J., Van Staal, C.R., and Rankin, D.W., 2007, A comparative analysis of pre-Silurian crustal building blocks of the northern and southern Appalachian orogen: American Journal of Science, v. 307, p. 23–45, https://doi.org/10.2475/01.2007.02.

Holland, T.J.B., and Powell, R., 1998, An internally consistent thermodynamic data set for phases of petrological interest: Journal of Metamorphic Geology, v. 16, p. 309–343, https://doi.org/10.1111/j.1525-1314.1998.00140.x.

Hopper, E., Fischer, K.M., Rondenay, S., Hawman, R.B., and Wagner, L.S., 2016, Imaging crustal structure beneath the Southern Appalachians with wavefield migration: Geophysical Research Letters, v. 43, p. 12,054–12,062, https://doi.org/10.1002/2016GL071005.

Huebner, M.T., Hatcher, R.D., Jr., and Merschat, A.J., 2017, Confirmation of the southwest continuation of the Cat Square terrane, Southern Appalachian Inner Piedmont, with implications for middle Paleozoic collisional orogenesis: American Journal of Science, v. 317, p. 95–176, https://doi.org/10.2475/02.2017.01.

Ingram, S., 2012, U-Pb Zircon and Monazite Geochronology and Hafnium Isotopic Geochemistry of Neoacadian and Early Alleghanian Plutonic Rocks in the Alabama Eastern Blue Ridge, Southern Appalachian Mountains [M.S. thesis]: Tuscaloosa, Alabama, University of Alabama.

Lee, C.T.A., Cheng, X., and Horodyskyj, U., 2006, The development and refinement of continental arcs by primary basaltic magmatism, garnet pyroxenite accumulation, basaltic recharge and delamination: Insights from the Sierra Nevada, California: Contributions to Mineralogy and Petrology, v. 151, p. 222–242, https://doi.org/10.1007/s00410-005-0056-1.

Ludwig, K., 2009, SQUID 2: A User's Manual, Rev. 12 April 2009: Berkeley Geochronology Center Special Publication 5, 110 p.

Ludwig, K.R., 2012, Isoplot 3.75: A Geochronological Toolkit for Microsoft Excel: Berkeley Geochronology Center Special Publication 5, 75 p.

Ma, C., Lin, Q., Mueller, P.A., Foster, D.A., Grimes, C.B., Heatherington, A.L., and Wooden, J.L., 2012, Alleghanian magmatism in the Southern Appalachians: Implications for the assembly of Pangea: Geological Society of America Abstracts with Programs, v. 44, no. 7, p. 571.

Mapes, R.W., 2002, Geochemistry and Geochronology of Mid-Palaeozoic Granitic Plutonism in the Southern Appalachian Piedmont Terrane, North Carolina–South Carolina–Georgia [M.S. thesis]: Nashville, Tennessee, Vanderbilt University.

McBride, J.H., and Nelson, K.D., 1991, Deep seismic reflection constraints on Paleozoic crustal structure and definition of the Moho in the buried southern Appalachian orogen, *in* Meissner, R., Brown, L., Dürbaum, H.J., Franke, W., Fuchs, K., and Seifert, F., eds., Continental Lithosphere: Deep Seismic Reflections: American Geophysical Union Geodynamics Monograph 22, p. 9–20.

McClellan, E.A., Steltenpohl, M.G., Thomas, C., and Miller, C.F., 2007, Isotopic age constraints and metamorphic history of the Talladega belt: New evidence for timing of arc magmatism and terrane emplacement along the southern Laurentian margin: The Journal of Geology, v. 115, p. 541–561, https://doi.org/10.1086/519777.

Merschat, A.J., Hatcher, R.D., Jr., and Davis, T.L., 2005, The northern Piedmont, USA: Kinematics of transpression and SW-directed mid-crustal flow: Journal of Structural Geology, v. 27, p. 1252–1281, https://doi.org/10.1016/j.jsg.2004.08.005.

Merschat, A.J., Bream, B.R., Huebner, M.T., Hatcher, R.D., Jr., and Miller, C.F., 2017, Temporal and spatial distribution of Paleozoic metamorphism in the Southern Appalachian Blue Ridge and Inner Piedmont delimited by ion microprobe U-Pb ages of metamorphic zircon, *in* Law, R., Thigpen, R., Merschat, A., and Stowell, H., eds., Linkages and Feedbacks in Orogenic Systems: Geological Society of America Memoir 213, p. 199–254, https://doi.org/10.1130/2017.1213(10).

Miller, B.V., Fetter, A.H., and Stewart, K.G., 2006, Plutonism in three orogenic pulses, eastern Blue Ridge Province, Southern Appalachians: Geological Society of America Bulletin, v. 118, p. 171–184, https://doi.org/10.1130/B25580.1.

Miller, C.F., Fullagar, P.D., Sando, T.W., Kish, S.A., Solomon, G.C., Russell, G.S., and Wood, L.F., 1997, Low-potassium, trondhjemitic to granodioritic plutonism in the eastern Blue Ridge, southwestern North Carolina–northeastern Georgia, *in* Sinha, A.K., Whalen, J.B., and Hogan, J.B., eds., The Nature of Magmatism in the Appalachian Orogen: Geological Society of America Memoir 191, p. 235–254, https://doi.org/10.1130/0-8137-1191-6.235.

Miller, C.F., Hatcher, R.D., Ayers, J.C., Coath, C.D., and Harrison, T.M., 2000, Age and zircon inheritance of eastern Blue Ridge plutons, southwestern North Carolina and northeastern Georgia, with implications for magma history and evolution of the southern Appalachian orogen: American Journal of Science, v. 300, p. 142–172, https://doi.org/10.2475/ajs.300.2.142.

Mueller, P., Kamenov, G., Heatherington, A., and Richards, J., 2008, Crustal evolution in the southern Appalachian orogen: Evidence from Hf isotopes in detrital zircons: The Journal of Geology, v. 116, p. 414–422, https://doi.org/10.1086/589311.

Neathery, T.L., and Reynolds, J.W., 1973, Stratigraphy and metamorphism of the Wedowee Group: A reconnaissance: American Journal of Science, v. 273, p. 723–741, https://doi.org/10.2475/ajs.273.8.723.

Nelson, K.D., 1992, Are crustal thickness variations in old mountain belts like the Appalachians a consequence of lithospheric delamination?: Geology, v. 20, p. 498–502, https://doi.org/10.1130/0091-7613(1992)020<0498:ACTVIO>2.3.CO;2.

Nelson, K.D., Arnow, J.A., McBride, J.H., Willemin, J.H., Huang, J., Zheng, L., Oliver, J.E., Brown, L.D., and Kaufman, S., 1985, New COCORP profiling in the southeastern United States. Part I: Late Paleozoic suture and Mesozoic rift basin: Geology, v. 13, p. 714–718, https://doi.org/10.1130/0091-7613(1985)13<714:NCPITS>2.0.CO;2.

Nelson, K.D., Arnow, J.A., Giguere, M., and Schamel, S., 1987, Normal-fault boundary of an Appalachian basement massif?: Results of COCORP profiling across the Pine Mountain belt in western Georgia: Geology, v. 15, p. 832–836, https://doi.org/10.1130/0091-7613(1987)15<832:NBOAAB>2.0.CO;2.

Pashin, J.C., 1994, Cycles and stacking patterns in Carboniferous rocks of the Black Warrior foreland basin: Gulf Coast Association of Geological Societies Transactions, v. 44, p. 555–563.

Pashin, J.C., and Gastaldo, R.A., 2009, Carboniferous of the Black Warrior Basin, *in* Greb, S.F., and Chestnut, D.R., Jr., eds., Carboniferous Geology and Biostratigraphy of the Appalachian and Black Warrior Basins: Kentucky Geological Survey Special Publication 1, Series 12, p. 10–21.

Russell, G.S., Odom, A.L., and Russell, C.W., 1987, Uranium-lead and rubidium-strontium isotopic evidence for the age and origin of granitic rocks in the northern Alabama Piedmont, *in* Drummond, M.S., and Green, N.L., eds., Granites of Alabama: Tuscaloosa, Alabama Geological Survey, p. 239–249.

Sacks, P.E., and Secor, D.T., 1990, Delamination in collisional orogens: Geology, v. 18, p. 999–1002, https://doi.org/10.1130/0091-7613(1990)018<0999:DICO>2.3.CO;2.

Samson, S.D., Coler, D.G., and Speer, J.A., 1995, Granites of the Southern Appalachians: Origin, tectonic setting: Earth and Planetary Science Letters, v. 134, p. 359–376, https://doi.org/10.1016/0012-821X(95)00124-U.

Schwartz, J.J., Johnson, K., Miranda, E.A., and Wooden, J.L., 2011, The generation of high Sr/Y plutons following Late Jurassic arc-arc collision, Blue Mountains province, NE Oregon: Lithos, v. 126, p. 22–41, https://doi.org/10.1016/j.lithos.2011.05.005.

Sinha, A.K., Hund, E.A., and Hogan, J.P., 1989, Paleozoic accretionary history of the North American plate margin (Central and Southern Appalachians): Constraints from the age, origin and distribution of granitic rocks, *in* Hillhouse, J.W., ed., Deep Structure and Past Kinematics of Accreted Terranes: American Geophysical Union Geophysical Monograph 50, p. 219–238.

Stacey, J.S., and Kramers, J.D., 1975, Approximation of terrestrial lead isotopic evolution by a two-stage model: Earth and Planetary Science Letters, v. 26, p. 207–221, https://doi.org/10.1016/0012-821X(75)90088-6.

Steltenpohl, M.G., ed., 2005, New Perspectives on Southernmost Appalachian Terranes, Alabama and Georgia: Tuscaloosa, Alabama Geological Society, 42nd Annual Field Trip Guidebook, 212 p.

Steltenpohl, M.G., Mueller, P.M., Heatherington, A.L., Hanley, T.B., and Wooden, J.L., 2008, Gondwanan/peri-Gondwanan origin for the Uchee terrane, Alabama and Georgia: Carolina zone or Suwannee terrane(?) and its suture with Grenvillian basement of the Pine Mountain window: Geosphere, v. 4, p. 131–144, https://doi.org/10.1130/GES00079.1.

Steltenpohl, M.G., Schwartz, J.J., and Miller, B.V., 2013, Late to post-Appalachian strain partitioning and extension in the Blue Ridge of Alabama and Georgia: Geosphere, v. 9, no. 3, p. 647–666, https://doi.org/10.1130/GES00738.1.

Stowell, H.H., and Odom Parker, K., 2015, The Hog Mountain Pluton, Alabama, *in* Stowell, H., Odom Parker, K., and Madden, J., eds., Neoacadian and Alleghanian Intrusion, Metamorphism, and Gold Mineralization in the Eastern Blue Ridge: Tuscaloosa, Alabama Geological Society, Guidebook for the 52nd Annual Field Trip, p. 11–37.

Stowell, H.H., Lesher, C.M., Green, N.L., Sha, P., Guthrie, G.M., and Sinha, A.K., 1996, Metamorphism and gold mineralization in the Blue Ridge, southernmost Appalachians: Economic Geology, v. 91, p. 1115–1144, https://doi.org/10.2113/gsecongeo.91.6.1115.

Stowell, H.H., Tulloch, A., Zuluaga, C.A., and Koenig, A., 2010, Timing and duration of garnet granulite metamorphism in magmatic arc crust, Fiordland, New Zealand: Chemical Geology, v. 273, p. 91–110, https://doi.org/10.1016/j.chemgeo.2010.02.015.

Stowell, H.H., Odom Parker, K., Gatewood, M.P., Tulloch, A., and Koenig, A., 2014, Temporal links between pluton emplacement, garnet granulite metamorphism, partial melting, and extensional collapse in the lower crust of a Cretaceous magmatic arc, Fiordland New Zealand: Journal of Metamorphic Geology, v. 32, p. 151–175, https://doi.org/10.1111/jmg.12064.

Thomas, W.A., 2004, Genetic relationship of rift-stage crustal structure, terrane accretion, and foreland tectonics along the southern Appalachian-Ouachita orogen: Journal of Geodynamics, v. 37, p. 549–563, https://doi.org/10.1016/j.jog.2004.02.020.

Thomas, W.A., 2011, The Iapetan rifted margin of southern Laurentia: Geosphere, v. 7, no. 1, p. 97–120, https://doi.org/10.1130/GES00574.1.

Tull, J.F., 1984, Polyphase late Paleozoic deformation in the southeastern foreland and northwestern Piedmont of the Alabama Appalachians: Journal of Structural Geology, v. 6, no. 3, p. 223–234, https://doi.org/10.1016/0191-8141(84)90047-6.

Tull, J.F., 1987, Structural setting of granitic plutonism in the Northern Piedmont, Alabama Appalachians, *in* Drummond, M.S., and Green, N.L., eds., Granites of Alabama: Tuscaloosa, Geological Survey of Alabama, p. 17–32.

Tull, J.F., Barineau, C.I., Mueller, P.A., and Wooden, J.L., 2007, Volcanic arc emplacement onto the southernmost Appalachian Laurentian shelf: Characteristics and constraints: Geological Society of America Bulletin, v. 119, no. 3–4, p. 261–274, https://doi.org/10.1130/B25998.1.

Tull, J.F., Mueller, P.A., and Barineau, C.I., 2009, Age and tectonic implications of the Elkahatchee Quartz Diorite, eastern Blue Ridge Province, Southern Appalachians, USA: Geological Society of America Abstracts with Programs, v. 41, no. 7, p. 288.

Tull, J.F., Holm-Denoma, C.S., and Barineau, C.I., 2014, Early to Middle Ordovician back-arc basin in the Southern Appalachian Blue Ridge: Characteristics, extent, and tectonic significance: Geological Society of America Bulletin, v. 126, p. 990–1015, https://doi.org/10.1130/B30967.1.

Tull, J.F., Mueller, P.A., Farris, D.W., and Davis, B.L., 2018, Taconic suprasubduction zone magmatism in southern Laurentia: Evidence from the Dadeville Complex: Geological Society of America Bulletin, v. 130, no. 7–8, p. 1339–1354, https://doi.org/10.1130/B31885.1.

Tulloch, A.J., and Kimbrough, D.L., 2003, Paired plutonic belts in convergent margins and the development of high Sr/Y magmatism: Peninsular Ranges Batholith of Baja-California and Median Batholith of New Zealand, *in* Johnson, S.E., Paterson, S.R., Fletcher, J.M., Girty, G.H., Kimbrough, D.L., and Martín-Barajas, A., eds., Tectonic Evolution of Northwestern Mexico and the Southwestern USA: Geological Society of America Special Paper 374, p. 275–296.

Uddin, A., Hames, W., Peavy, T., and Pashin, J., 2016, Detrital history of the Lower Pennsylvanian Pottsville Formation in the Cahaba synclinorium of Alabama, U.S.A.: Journal of Sedimentary Research, v. 86, p. 1287–1297, https://doi.org/10.2110/jsr.2016.76.

Vauchez, A., 1987, Brevard fault zone, Southern Appalachians: A medium-angle, dextral, Alleghanian shear zone: Geology, v. 15, p. 669–672, https://doi.org/10.1130/0091-7613(1987)15<669:BFZSAA>2.0.CO;2.

Vauchez, A., Babaie, H., and Babaei, A., 1993, Orogen-parallel tangential motion in the Late Devonian–early Carboniferous Southern Appalachian Internides: Canadian Journal of Earth Sciences, v. 30, p. 1297–1305, https://doi.org/10.1139/e93-111.

Vermeesch, P., 2018, IsoplotR: A free and open toolbox for geochronology: Geoscience Frontiers, v. 9, p. 1479–1493, https://doi.org/10.1016/j.gsf.2018.04.001.

Vervoort, J.D., and Blichert-Toft, J., 1999, Evolution of the depleted mantle: Hf isotope evidence from juvenile rocks through time: Geochimica et Cosmochimica Acta, v. 63, p. 533–556, https://doi.org/10.1016/S0016-7037(98)00274-9.

Xu, W.-C., Zhang, H.-F., Guo, L., and Yuan, H.-L., 2010, Miocene high Sr/Y magmatism, south Tibet: Product of partial melting of subducted Indian continental crust and its tectonic implication: Lithos, v. 114, p. 293–306, https://doi.org/10.1016/j.lithos.2009.09.005.

Zeng, L., Gao, L.E., Xie, K., and Liu-Zeng, J., 2011, Mid-Eocene high Sr/Y granites in the northern Himalayan gneiss domes: Melting thickened lower continental crust: Earth and Planetary Science Letters, v. 303, p. 251–266, https://doi.org/10.1016/j.epsl.2011.01.005.

MANUSCRIPT RECEIVED 12 NOVEMBER 2018
REVISED MANUSCRIPT RECEIVED 24 MAY 2019
MANUSCRIPT ACCEPTED 28 JUNE 2019